

## Structure-based design of inhibitors selective for human proteasome #2c or #2i subunits

Bo-Tao Xin, Eva Huber, Gerjan de Bruin, Wolfgang Heinemeyer, Elmer Maurits, Christopher Espinal, Yimeng Du, Marissa Janssens, Emily S. Weyburne, Alexei Kisselev, Bogdan I. Florea, Christoph Driessen, Gijsbert A. van der Marel, Michael Groll, and Herman S. Overkleeft

*J. Med. Chem.*, **Just Accepted Manuscript** • DOI: 10.1021/acs.jmedchem.8b01884 • Publication Date (Web): 18 Jan 2019

Downloaded from <http://pubs.acs.org> on January 18, 2019

### Just Accepted

"Just Accepted" manuscripts have been peer-reviewed and accepted for publication. They are posted online prior to technical editing, formatting for publication and author proofing. The American Chemical Society provides "Just Accepted" as a service to the research community to expedite the dissemination of scientific material as soon as possible after acceptance. "Just Accepted" manuscripts appear in full in PDF format accompanied by an HTML abstract. "Just Accepted" manuscripts have been fully peer reviewed, but should not be considered the official version of record. They are citable by the Digital Object Identifier (DOI®). "Just Accepted" is an optional service offered to authors. Therefore, the "Just Accepted" Web site may not include all articles that will be published in the journal. After a manuscript is technically edited and formatted, it will be removed from the "Just Accepted" Web site and published as an ASAP article. Note that technical editing may introduce minor changes to the manuscript text and/or graphics which could affect content, and all legal disclaimers and ethical guidelines that apply to the journal pertain. ACS cannot be held responsible for errors or consequences arising from the use of information contained in these "Just Accepted" manuscripts.



# Structure-based design of inhibitors selective for human proteasome $\beta$ 2c or $\beta$ 2i subunits

*Bo-Tao Xin<sup>†,1</sup>, Eva M. Huber<sup>§,1</sup>, Gerjan de Bruin<sup>†</sup>, Wolfgang Heinemeyer<sup>§</sup>, Elmer Maurits<sup>†</sup>, Christofer Espinal<sup>†</sup>, Yimeng Du<sup>†</sup>, Marissa Janssens<sup>†</sup>, Emily S. Weyburne<sup>#</sup>, Alexei F. Kisselev<sup>#&</sup>, Bogdan I. Florea<sup>†</sup>, Christoph Driessen<sup>†</sup>, Gijsbert A. van der Marel<sup>†</sup>, Michael Groll<sup>§,\*</sup> and Herman S. Overkleeft<sup>†,\*</sup>*

<sup>†</sup>Gorlaeus Laboratories, Leiden Institute of Chemistry and Netherlands Proteomics Centre, Einsteinweg 55, 2333 CC Leiden, The Netherlands

<sup>§</sup>Center for Integrated Protein Science at the Department Chemie, Lehrstuhl für Biochemie, Technische Universität München, 85748 Garching, Germany

<sup>‡</sup>Department of Hematology and Oncology, Kantonsspital St. Gallen, 9007 St. Gallen, Switzerland

<sup>#</sup>Department of Molecular and Systems Biology and Norris Cotton Cancer Center, Geisel School of Medicine at Dartmouth, 1 Medical Centre Drive HB7936, Lebanon, New Hampshire 03756, United States of America.

\*To whom correspondence should be addressed.

<sup>&</sup>Current address: Department of Drug Discovery and Development, Harrison School of Pharmacy, Auburn University, Auburn AL 36849 USA

<sup>1</sup>These authors contributed equally.

KEYWORDS Constitutive proteasome, immunoproteasome, epoxyketone, vinyl sulfone, subunit selectivity, ligand binding

## ABSTRACT

Subunit-selective proteasome inhibitors are valuable tools to assess the biological and medicinal relevance of individual proteasome active sites. While inhibitors for the  $\beta 1c$ ,  $\beta 1i$ ,  $\beta 5c$  and  $\beta 5i$  subunits exploit differences in the substrate binding channels identified by X-ray crystallography, compounds selectively targeting  $\beta 2c$  or  $\beta 2i$  could not yet be rationally designed due to the high structural similarity of these two subunits. Here we report the development, chemical synthesis and biological screening of a compound library that led to the identification of the  $\beta 2c$ - and  $\beta 2i$ -selective compounds LU-002c (**4**;  $IC_{50} \beta 2c$ : 8 nM,  $IC_{50} \beta 2i/\beta 2c$ : 20-fold) and LU-002i (**5**;  $IC_{50} \beta 2i$ : 220 nM,  $IC_{50} \beta 2c/\beta 2i$ : 45-fold), respectively. Co-crystal structures with  $\beta 2$ -humanized yeast proteasomes visualize protein-ligand interactions crucial for subunit specificity. Altogether, organic syntheses, activity-based protein profiling, yeast mutagenesis and structural biology allowed us to decipher significant differences of  $\beta 2$  substrate binding channels and to complete the set of subunit-selective proteasome inhibitors.

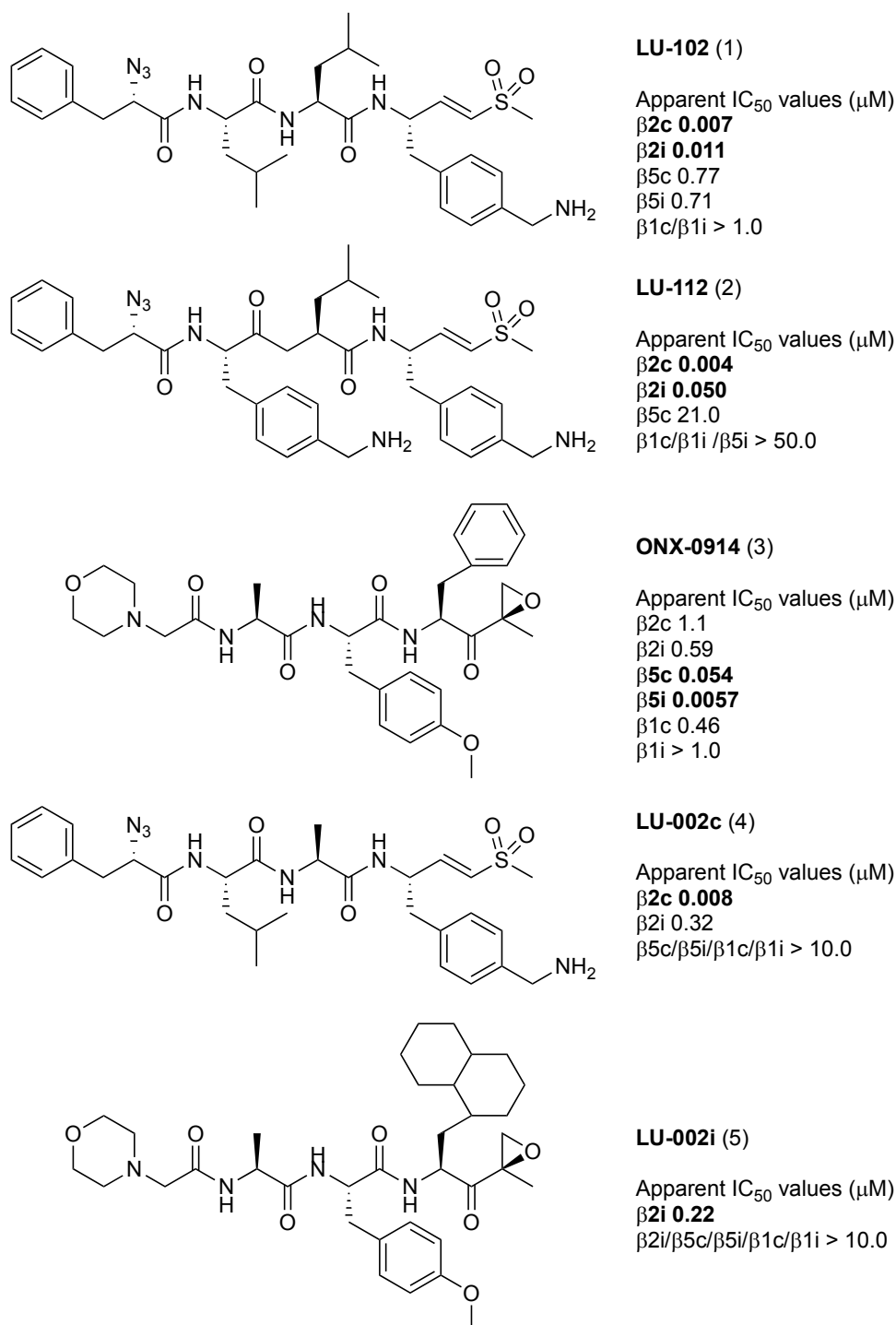
## Introduction

Proteasomes are proteolytic machines responsible for the degradation of misfolded proteins localized in the cytosol and nucleus of eukaryotic cells<sup>1</sup>. Their 20S core particles (CPs) are C2-symmetrical barrel-shaped complexes assembled of 28 subunits that are arranged in four stacked seven-membered rings<sup>2</sup>. The two outer rings are made of seven  $\alpha$ -subunits ( $\alpha$ 1-7) and the two inner rings consist of seven homologous yet distinct  $\beta$ -subunits ( $\beta$ 1-7). In ubiquitously expressed constitutive proteasomes (cCPs), the proteolytic activities reside within the subunits  $\beta$ 1c (caspase-like activity),  $\beta$ 2c (trypsin-like activity) and  $\beta$ 5c (chymotrypsin-like activity)<sup>3</sup>. In lymphoid-tissues these subunits are replaced by their interferon- $\gamma$ -inducible counterparts,  $\beta$ 1i (LMP2),  $\beta$ 2i (MECL-1) and  $\beta$ 5i (LMP7)<sup>4</sup>, yielding so-called immunoproteasome particles (iCPs) that preferentially generate antigenic peptides with high affinity for major histocompatibility complex (MHC) class I receptors<sup>5</sup>.

Proteasomes are validated drug targets in oncology and numerous, structurally diverse inhibitors of natural and non-natural origin have been reported so far<sup>6</sup>. Most synthetic compounds are N-terminally capped peptides of 2-4 residues with a C-terminal electrophilic warhead that forms a covalent linkage with the nucleophilic hydroxyl group and possibly the free N-terminus of threonine-1 (Thr1) of catalytically active proteasomal  $\beta$ -subunits<sup>7</sup>. Subunit specificity of peptidic ligands is largely determined by the sequence of the peptide fragment, although the nature of the warhead can confer selectivity as well<sup>8</sup>. The first generation boronic acid bortezomib and the second generation epoxyketone carfilzomib target more than one subunit at a time and therefore are considered broad-spectrum proteasome inhibitors<sup>6a</sup>. Bortezomib and carfilzomib are now approved drugs for the treatment of multiple myeloma<sup>9,10</sup>. Current industrial and academic drug design efforts focus on the development of subunit-selective proteasome inhibitors and their

potential therapeutic use in chronic inflammatory diseases. For instance, the first immunoproteasome-selective compound KZR-616<sup>11</sup>, an analog of ONX 0914<sup>12</sup>, has recently entered phase 1b/2 clinical trials for the treatment of lupus erythematosus. Besides medical issues, selective inhibition of individual proteasome subunits may aid investigations on the involvement of these sites in different cellular pathways including MHC class I antigen presentation and control of cytokine levels. Although there is an overlap in the substrate preferences of cCP and iCP subunits, distinct structural features and amino acid linings of the substrate binding channels  $\beta 1c$  and  $\beta 1i$  as well as  $\beta 5c$  and  $\beta 5i$  could be identified and subsequently allowed for the development of specific inhibitors<sup>12-13</sup>. Design of inhibitors targeting exclusively  $\beta 2c$  or  $\beta 2i$  however remained challenging due to the high structural similarity between the trypsin-like active sites<sup>13d</sup>. In 2018, Liskamp and co-workers reported a set of  $\beta 2$ -selective inhibitors. However, these compounds, which are characterized by a sulfonyl fluoride as the C-terminal electrophile, a basic P1 residue and a free N-terminus, display limited preference for either  $\beta 2c$  or  $\beta 2i$ .<sup>14</sup> As well, Kezar Life Sciences developed a epoxyketone inhibitor with moderate selectivity for human  $\beta 2i$ <sup>11</sup>.

Recently, we published a set of activity-based protein profiling (ABPP) probes and inhibitors selective for each of the six catalytic activities of human cCP and iCP, including compounds LU-002c ( $\beta 2c$ ) and LU-002i ( $\beta 2i$ ; Figure 1)<sup>15</sup>. Here, we describe the design, synthesis and screening of focused compound libraries that allowed us to identify these  $\beta 2c$  and  $\beta 2i$  inhibitors, respectively. Crystallographic data on humanized yeast proteasomes in complex with selective ligands provide insights into their mode of binding and reveal so far unnoticed differences in substrate and inhibitor specificity for the trypsin-like active sites of cCP and iCP.



**Figure 1.** Chemical structures and IC<sub>50</sub> values for the lead structures LU-102 (1)<sup>16</sup>, LU-112 (2)<sup>16</sup> and ONX 0914 (3)<sup>12</sup> that guided the development of the β2c- and β2i-selective compounds LU-002c (4) and LU-002i (5), respectively. IC<sub>50</sub> values were measured by competitive ABPP.

## Results

### Development of selective inhibitors for subunit $\beta 2c$

The previously identified vinyl sulfone inhibitor LU-102 (Figure 1), which inhibits  $\beta 2c$  and  $\beta 2i$  with similar potency<sup>16</sup>, was used as a starting point for creating selective  $\beta 2c$  ligands. We generated a compound library based on the vinyl sulfone warhead and the 4-aminomethylphenyl side chain on P1 of LU-102, as these moieties proved to be crucial for  $\beta 2$ -selectivity in general<sup>16</sup>. In a first step, we replaced the N-cap of LU-102 by a set of groups often found in peptide-based proteasome inhibitors (**6-12**). Next, we synthesized compounds with relatively small amino acid side chains in the P2 position (**4**, **13-20**) and finally incorporated bulky aliphatic side chains at P2 and P3 (**21-36**). In total, 32 compounds were prepared using established protocols for the chemical synthesis of the 4-aminomethylphenylalanine vinyl sulfone warhead and solution-phase coupling of the peptide vinyl sulfones to the corresponding  $\alpha$ -amino acids (see Supporting Information)<sup>27</sup>.

All compounds were evaluated for  $\beta 2c/\beta 2i$  inhibition by our competitive ABPP assay at final concentrations of 0.01, 0.1, 1.0 as well as 10.0  $\mu$ M and apparent  $IC_{50}$  values were determined (Table 1). Among the N-cap series **6-12**, compound **7** (pyrazine N-cap) showed the highest selectivity for  $\beta 2c$  over  $\beta 2i$  (40-fold), but also decreased potency for  $\beta 2c$  compared to LU-102 (23-fold). Screening of small P2 residues (compounds **4**, **13-20**) identified several ligands with both good selectivity and potency for  $\beta 2c$ : **4** (P2 alanine; 10 nM, 32-fold selectivity over  $\beta 2i$ ), **13** (P2 serine; 11 nM, 47-fold), **15** (P2 methoxyserine; 8 nM, 25-fold), **16** (P2 threonine; 8 nM, 41-fold) and especially **18** (P2 glycine; 26 nM, 224-fold). Combining 2-methylthiazole N-caps (**20**) with bulky P2 or P3 residues (**21-36**) revealed several potent and selective  $\beta 2c$  compounds, as well: see for instance, compounds **20** (P2 methoxyserine, P3 leucine; 72 nM, 14-fold), **22** (P2

leucine, P3 cyclohexyl; 18 nM, 30-fold), **30** (P2 cyclohexyl-homoalanine, P3 leucine; 11 nM, 25-fold) and **36** (P2 and P3 cyclohexyl 40 nM, 10.5-fold). Altogether, based on the data shown in Table 1 we conclude that 1) subunit  $\beta$ 2c accepts small as well as bulky P2 residues but disfavors oversized P3 side chains; and 2) that  $\beta$ 2i disfavors small P2 side chains and large P3 groups.

To establish apparent  $IC_{50}$  values more accurately and to obtain insights into co-inhibition of  $\beta$ 1c,  $\beta$ 1i,  $\beta$ 5c and  $\beta$ 5i activities, we selected the compounds **4**, **7**, **13**, **16**, **18**, **20**, **22** and **25** for further analysis. In our competitive ABPP assay using Raji cell extracts (containing both cCPs and iCPs) a wider range of final concentrations were tested. All compounds inhibited  $\beta$ 2c at low nanomolar concentrations (Table 2). Inhibitors **4**, **13**, **18** and **20**, featuring small side chains on P2, displayed considerably enhanced selectivity for  $\beta$ 2c over  $\beta$ 2i ( $\geq 27$ -fold) compared to LU-102 (1.6-fold; Table 2) with **18** being the most selective (54-fold).

Next, we assessed the inhibitory effects in living RPMI-8226 cells (Table 3). Initial screenings identified compound **4** as the most active, and we included this compound as LU-002c in our suite of subunit-selective proteasome inhibitors<sup>15</sup>. In subsequent studies we identified compound **16** to be even more potent and selective and we dubbed this compound LU-012c.

### Development of $\beta$ 2i-selective inhibitors

For the development of  $\beta$ 2i-selective compounds, we used ONX 0914 (**3**)<sup>12</sup> as starting point (Figure 1). Though ONX 0914 is a  $\beta$ 5i selective inhibitor, it also targets other proteasome subunits<sup>12, 13b</sup> (Figure 1) and shows slight selectivity for  $\beta$ 2i over  $\beta$ 2c ( $IC_{50}$  ( $\beta$ 2i) 0.59  $\mu$ M;  $IC_{50}$  ( $\beta$ 2c) 1.1  $\mu$ M, 1.9-fold)<sup>13b</sup>. During our efforts to create  $\beta$ 5i-selective compounds, we noted that substitution of the P1 phenylalanine in ONX 0914 for cyclohexylalanine enhances selectivity for both  $\beta$ 5i and  $\beta$ 2i over the respective constitutive subunits (ratio  $\beta$ 2c/ $\beta$ 2i = 6) and that any additional modifications of the P2 and P3 positions as well as the N-cap led to the loss of activities for the trypsin-like sites<sup>13b</sup>. Based on these observations, we reasoned that large

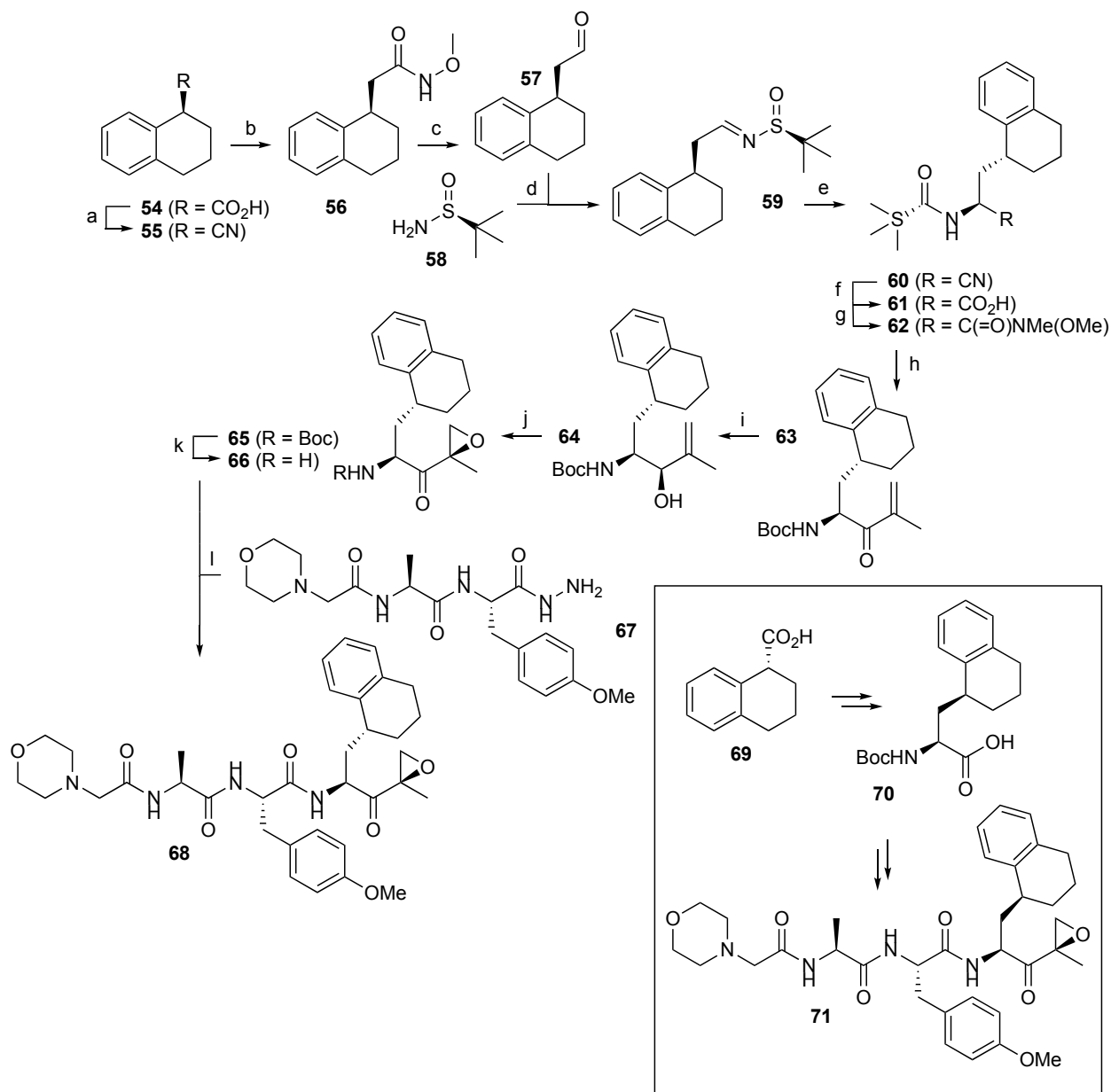


aliphatic amino acid residues at P1 might lead to  $\beta$ 2i selective inhibitors. To probe this hypothesis, a set of epoxyketone inhibitors with large hydrophobic P1 residues (compounds **5**, **37-53**, Table 4) was synthesized (for details see Supporting Information).

The compounds were tested at final concentrations of 0.01, 0.1, 1.0 and 10.0  $\mu$ M by our competitive ABPP assay and apparent  $IC_{50}$  values for inhibition of  $\beta$ 2c and  $\beta$ 2i were determined (Table 4). In this first evaluation step, compounds **5** (P1 1-decalanine; 319 nM, >31-fold), **39** (P1 cyclohexyl-homoalanine; 215 nM, >46-fold), **41b** (methylcyclohexylalanine, 264 nM, 24-fold) and **44b** (bicyclohexylalanine, 97 nM, 9-fold) showed the highest selectivity for  $\beta$ 2i over  $\beta$ 2c.

Next, inhibition of all six sites by compounds **5** and **39** were tested at a wider range of final concentrations (Table 5). In this set-up, compound **5** proved to be the most selective  $\beta$ 2i ligand (ratio  $\beta$ 2c/ $\beta$ 2i: 67) as it did not inhibit any of the  $\beta$ 1 and  $\beta$ 5 proteasome subunits. By contrast, epoxyketone **39** proved to be a dual inhibitor of both  $\beta$ 2i and  $\beta$ 5i with high selectivity over the corresponding constitutive subunits (ratio  $\beta$ 2c/ $\beta$ 2i: 44; ratio  $\beta$ 5c/ $\beta$ 5i: 109).

Epoxyketone **5**, the most selective  $\beta$ 2i-inhibitor of the series, was termed LU-002i and published as part of a set of compounds and ABPP probes to visualize all six catalytic activities of human constitutive and immunoproteasomes<sup>15</sup>. However, the decalin moiety of **5** was synthesized as a mixture of stereoisomers that could not be separated. To address the question whether one or both of the possible stereomers are active, the following attempts were undertaken to synthesize a stereomerically pure analogue of **5** (LU-002i). First, compounds with partially reduced naphthyl rings containing only one chiral carbon center within the bicyclic system were synthesized: **68** (*R*) and **71** (*S*) (Scheme 1; Supporting Information). In the competitive ABPP assay in Raji cell lysates (Table 6) **68** was inactive, while **71** selectively targeted  $\beta$ 2i though with dramatic loss of potency ( $IC_{50}$  2.54  $\mu$ M) compared to **5** ( $IC_{50}$  0.18  $\mu$ M).

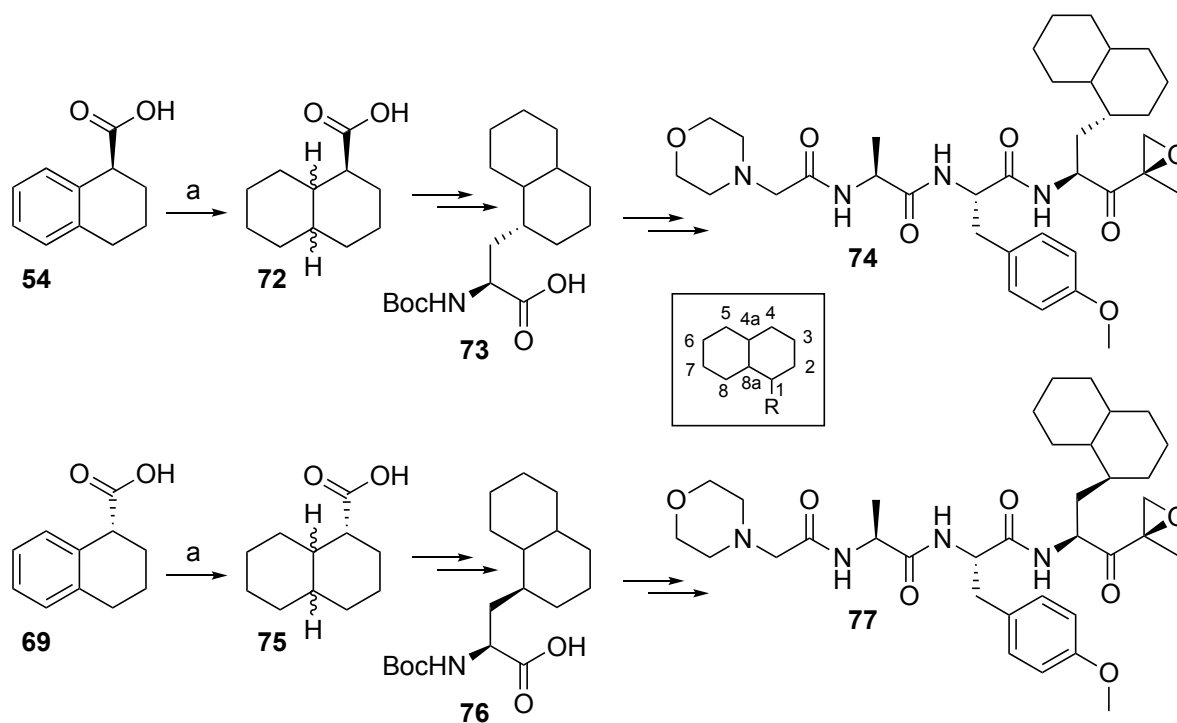
**Scheme 1.** Synthesis of compounds **68** and **71**.

Reagents and conditions: (a) i) LiAlH<sub>4</sub>/Et<sub>2</sub>O, 99%; ii) TsCl/TEA/DCM, 97%; iii) NaCN/DMF, 95%; (b) i) KOH/ethylene glycol; ii) *N,O*-dimethylhydroxylamine hydrochloride, HCTU/DiPEA/DCM, 49% over two steps; (c) LiAlH<sub>4</sub>/Et<sub>2</sub>O; (d) **58**/CuSO<sub>4</sub>/DCM, 84% two-step yield; (e) Et<sub>2</sub>AlCN/*i*-PrOH/THF, 58%; (f) i) 6 M HCl, reflux; ii) Boc<sub>2</sub>O/TEA/THF/H<sub>2</sub>O, 58% over two steps; (g) *N,O*-dimethylhydroxylamine hydrochloride, HCTU/DiPEA/DCM, 77%; (h)

*t*BuLi/2-bromopropene/Et<sub>2</sub>O, -78 °C, 78%; (i) NaBH<sub>4</sub>/CeCl<sub>3</sub>·7H<sub>2</sub>O/MeOH, 59%; (j) 1) VO(acac)<sub>2</sub>/*t*BuOOH /DCM; 2) Dess-Martin periodinane/DCM, 33% over two steps; (k) TFA, quantitative yield; (l) 1) **67**, *t*BuONO/HCl (4N in dioxane) DCM/DMF, -30 °C; 2) **66**, DiPEA, DMF, 40% over two steps.

In a second approach to unravel the active stereomer of **5**, fully reduced decaline systems were produced, yielding the peptide epoxyketones **74** and **77**, respectively (Scheme 2, Supporting Information). Competitive ABPP revealed that **74** inhibits β<sub>2</sub>i with an IC<sub>50</sub> of 12.0 μM without touching the other five active sites of cCP and iCP particles (Table 6). Compound **77** in turn proved to be a potent β<sub>2</sub>i inhibitor (IC<sub>50</sub> 0.384 μM) with some cross reactivity against β<sub>2</sub>c (IC<sub>50</sub> 27.64 μM). Notably, the absolute stereochemistry of the P1 side chain in **77** matches that of the corresponding carbon center in ligand **71**, but it appears that a decaline at P1 (**77**) is more effective for β<sub>2</sub>i inhibition than the corresponding partially oxidized bicyclic system (**71**).

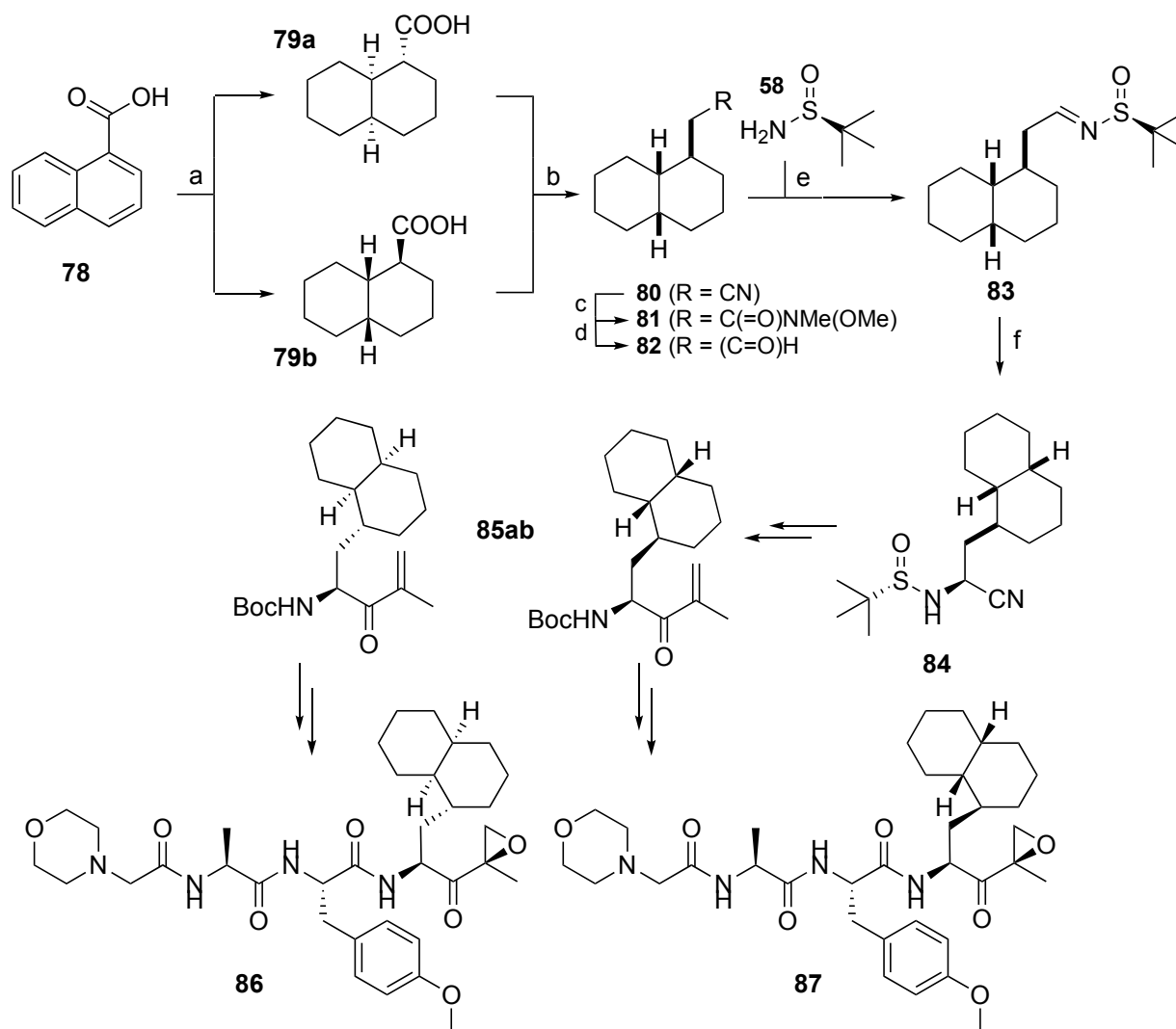
**Scheme 2.** Synthesis of compounds **74** and **77**.



Reagents and conditions: (a) H<sub>2</sub>, PtO<sub>2</sub>, AcOH, 99%.

With this information in hand, an enantiomerically pure diastereomeric set of peptide epoxyketones **86** and **87** was synthesized (Scheme 3; Supporting Information). Compound **86** appeared to be a weak (IC<sub>50</sub> 33.71 μM) but selective β<sub>2</sub>i inhibitor, whereas epoxyketone **87** strongly inhibits β<sub>2</sub>i (IC<sub>50</sub> 0.189 μM) with β<sub>2</sub>c, β<sub>1</sub>c and β<sub>5</sub>i as off targets at high micromolar concentrations (Table 6). Based on the assumption that carbon 1 in the decaline system of compound **87** has the (*S*) configuration as in **71** and **77**, and assuming that the catalytic hydrogenation proceeded to deliver the decaline with *cis,cis* stereochemistry, the observed results strongly suggest that the stereochemistry of the most active and selective β<sub>2</sub>i-inhibitor is as shown in structure **87** (Scheme 3).

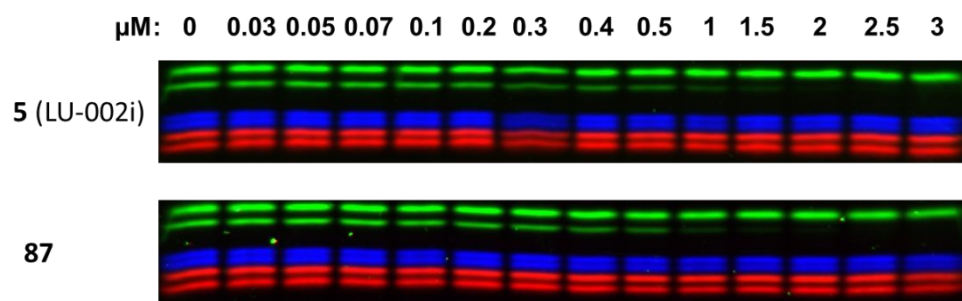
**Scheme 3.** Synthesis of compounds **86** and **87**.



Reagents and conditions: (a)  $\text{H}_2$ ,  $\text{PtO}_2$ , AcOH, quantitative yield; (b) i)  $\text{LiAlH}_4/\text{Et}_2\text{O}$ , 92%; ii)  $\text{TsCl}/\text{TEA}/\text{DCM}$ , 95%; 3)  $\text{NaCN}/\text{DMF}$ , 83%; (c) i)  $\text{KOH}/\text{ethylene glycol}$ ; ii) *N,O*-dimethylhydroxylamine hydrochloride, HCTU/DiPEA/DCM, 88% over two steps; (d)  $\text{LiAlH}_4/\text{Et}_2\text{O}$ ; (e) **58**/ $\text{CuSO}_4/\text{DCM}$ , 85% over two steps; (f)  $\text{Et}_2\text{AlCN}/i\text{-PrOH}/\text{THF}$ , 75%.

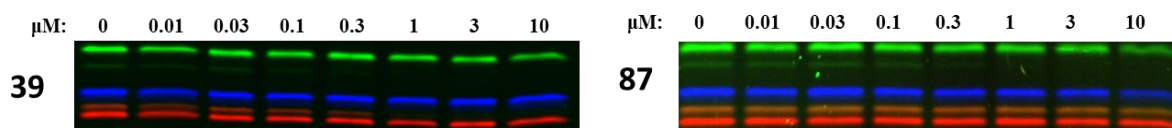
To test whether compound **87** is the major active component of the stereomeric mixture that makes up compound **5** (the previously described  $\beta 2\text{i}$ -selective inhibitor, LU-002i<sup>15</sup>) both were assessed in a competitive ABPP assay in Raji cell extracts at final inhibitor concentrations ranging from 0 to 3  $\mu\text{M}$  (Figure 2). Since both preparations are about equally active and selective,

diastereomer **87** appears to be indeed the main active component in the stereomeric mixture that has previously been reported as LU-002i<sup>15</sup>.



**Figure 2.** Comparative activity-based protein profiling assay of compounds **5** (LU-002i) and **87**, determined in Raji cell lysates.

Next, compound **87** was tested in intact RPMI-8226 cell lines, in comparison with the dual  $\beta$ 2i/ $\beta$ 5i inhibitor **39**. Cells were first treated with inhibitor at various concentrations, then lysed, incubated with the ABPP mixture, denatured and resolved on SDS PAGE as described before. Like in Raji cell lysates, compound **87** selectively targeted only  $\beta$ 2i ( $IC_{50}$  0.159  $\mu$ M) without affecting the remaining proteolytically active proteasome subunits, whereas epoxyketone **39** inhibited both  $\beta$ 2i ( $IC_{50}$  0.124  $\mu$ M) and  $\beta$ 5i ( $IC_{50}$  0.183  $\mu$ M) (Figure 3). Thus, inhibitor **39** represents a co-inhibitor of  $\beta$ 2i and  $\beta$ 5i with potential medicinal relevance, especially because targeting of  $\beta$ 2 has previously been shown to sensitize cells to  $\beta$ 5 inhibitors<sup>17</sup> and dual subunit inhibition is required for suppressing autoinflammatory reactions<sup>11</sup>.

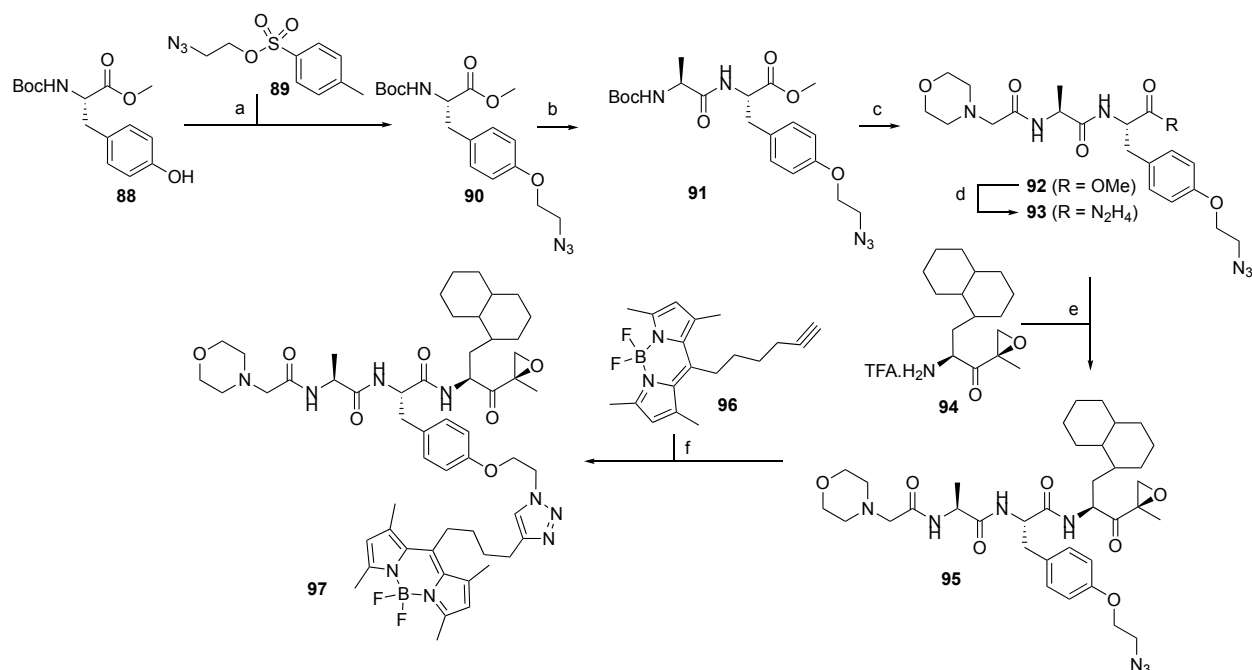


**Figure 3.** Inhibition profiles of compounds **39** and **87**, determined in intact RPMI-8226 cell lines.

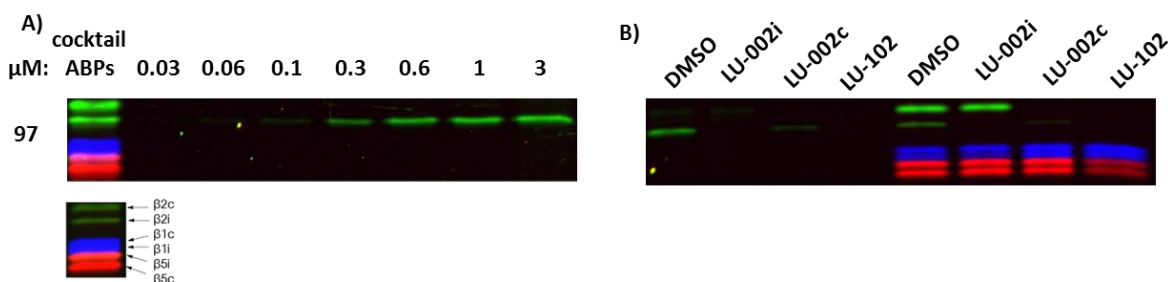
As the next research objective we decided to investigate whether a  $\beta$ 2i-selective activity-based probe could be derived from LU-002i (**5**). Since attachment of a fluorescent tag at the N-terminus of subunit-selective inhibitors may be detrimental to selectivity, we decided to graft the

reporter group onto the tyrosine residue at P2 by substituting the methyl group for an appropriately functionalized alkyl group (Scheme 4). The resulting activity-based probe **97** was tested in Raji cell lysate to profile the proteasome activities. At a final concentration of 3  $\mu$ M,  $\beta$ 2i-labeling was selective and could be easily distinguished (Figure 4A). In a competitive ABPP assay with probe **97** labeling of  $\beta$ 2i could be completely abolished by pre-incubation with LU-002i (**5**,  $\beta$ 2i) at 3  $\mu$ M. The  $\beta$ 2i signal was partially reduced after treatment with LU-002c (**4**,  $\beta$ 2c) at high concentrations, and completely abolished after pre-incubation with LU-102 (**1**,  $\beta$ 2c/ $\beta$ 2i) (Figure 4B). Finally, a competitive ABPP assay with probe **97** side-by-side with the three-probe mixture used previously in competitive ABPP experiments was carried out. This time treatment with LU-002i (**5**,  $\beta$ 2i) selectively blocked  $\beta$ 2i-labeling by the three probes at 3  $\mu$ M, whereas LU-002c (**4**,  $\beta$ 2c) completely prevented  $\beta$ 2c identification (0.3  $\mu$ M final concentration) and partially inhibited  $\beta$ 2i labeling. Furthermore, LU-102 (**1**,  $\beta$ 2c/ $\beta$ 2i) blocked both  $\beta$ 2c- and  $\beta$ 2i- labeling at 1  $\mu$ M (Figure 4B). These results match those published earlier on these compounds against the same set of probes<sup>15</sup>. Altogether these data demonstrates that ABP **97** is a potent and highly selective ABP for visualizing  $\beta$ 2i activities of human immunoproteasomes.

**Scheme 4.** Synthesis of probe **97**.



Reagents and conditions: (a) **89**,  $\text{K}_2\text{CO}_3/\text{DMF}$ , 80%; (b) i) TFA, 99%; ii) Boc-Ala-OH, HCTU/DiPEA/DCM, 93%; (c) i) TFA, 99%; ii) 2-morpholino acetic acid, HCTU/DiPEA/DCM, 32%; (d)  $\text{N}_2\text{H}_4 \cdot \text{H}_2\text{O}$ , MeOH, 99%; (e)  $t\text{BuONO}/\text{HCl}$  (4N in dioxane), DCM/DMF (1/1, v/v),  $-30^\circ\text{C}$ , 56%; (f)  $\text{CuSO}_4$ , sodium ascorbate, DMF, 18%.



**Figure 4.** (A) Activity-based proteasome profiling using probe **97** at different concentrations. Cocktail ABPs were added as control. (B) Left: Competitive activity-based protein profiling assay using ABP **97** and the inhibitors **1** (LU-102, 0.1  $\mu\text{M}$ ), **4** (LU-002c, 0.03  $\mu\text{M}$ ) and **5** (LU-002i, 0.1  $\mu\text{M}$ ). Right: Competitive ABPP assay with probe **97** side-by-side with the three-probe



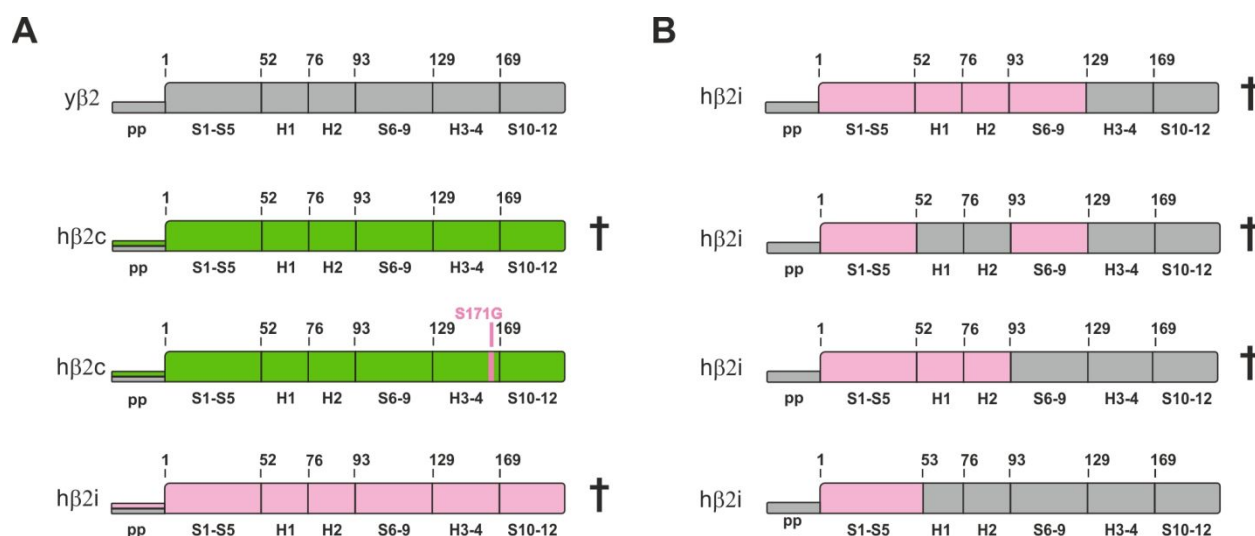
mixture used previously in competitive ABPP experiments and the inhibitors **1** (LU-102, 0.1  $\mu$ M), **4** (LU-002c, 0.03  $\mu$ M) and **5** (LU-002i, 0.1  $\mu$ M).

### **X-ray structures of selected inhibitors in complex with yeast and humanized CPs**

In order to obtain more insights into the structural features that drive either  $\beta$ 2c- or  $\beta$ 2i-selectivity of ligands, we aimed at determining X-ray structures of selected compounds in complex with CPs. Since structural data on the human apo iCP are not available, we recently developed chimeric yeast proteasomes, which feature key elements of human  $\beta$ 5 subunits, as structural tools<sup>18</sup>. Based on this work, we here created  $\beta$ 2 humanized yeast proteasomes.

While yeast proteasome  $\alpha$  subunits can be easily exchanged by human counterparts, replacement of most  $\beta$  entities i.e.  $\beta$ 1,  $\beta$ 2,  $\beta$ 5,  $\beta$ 6 and  $\beta$ 7 is lethal to yeast<sup>13d, 18-19</sup>. Strikingly however, the single point mutation S171G suffices to rescue the lethal phenotype that is caused by substitution of the endogenous yeast (y)  $\beta$ 2 subunit with the human (h)  $\beta$ 2c counterpart<sup>19</sup>. We created the respective  $\beta$ 2c chimeric yeast strain (Figures 5A, S8), purified and crystallized its mutant proteasome. The X-ray structure (Table S13) revealed that the  $\beta$ 2 propeptide was released from the active site Thr1 and that the overall fold of the subunit was intact (Figure 6A). Although the S171G mutation had no obvious impact on the structure of the matured mutant proteasome, it likely supports subunit folding and proteasome assembly. Any pronounced effects of Gly171 on  $\beta$ 2 activity are excluded, as yeast viability does not depend on peptide bond hydrolysis by  $\beta$ 2<sup>20</sup>.

Since no rescuing mutation for the h $\beta$ 2i subunit is known to date, we created various chimeric h $\beta$ 2i-y $\beta$ 2 constructs and tested whether they can substitute wild-type (WT) y $\beta$ 2. Surprisingly, only a construct featuring the  $\beta$ 2i amino acids 1-53 was viable (Figure 5B). As this sequence covers the entire  $\beta$ 2 substrate binding channel, we used this construct for structural analyses (Table S13).

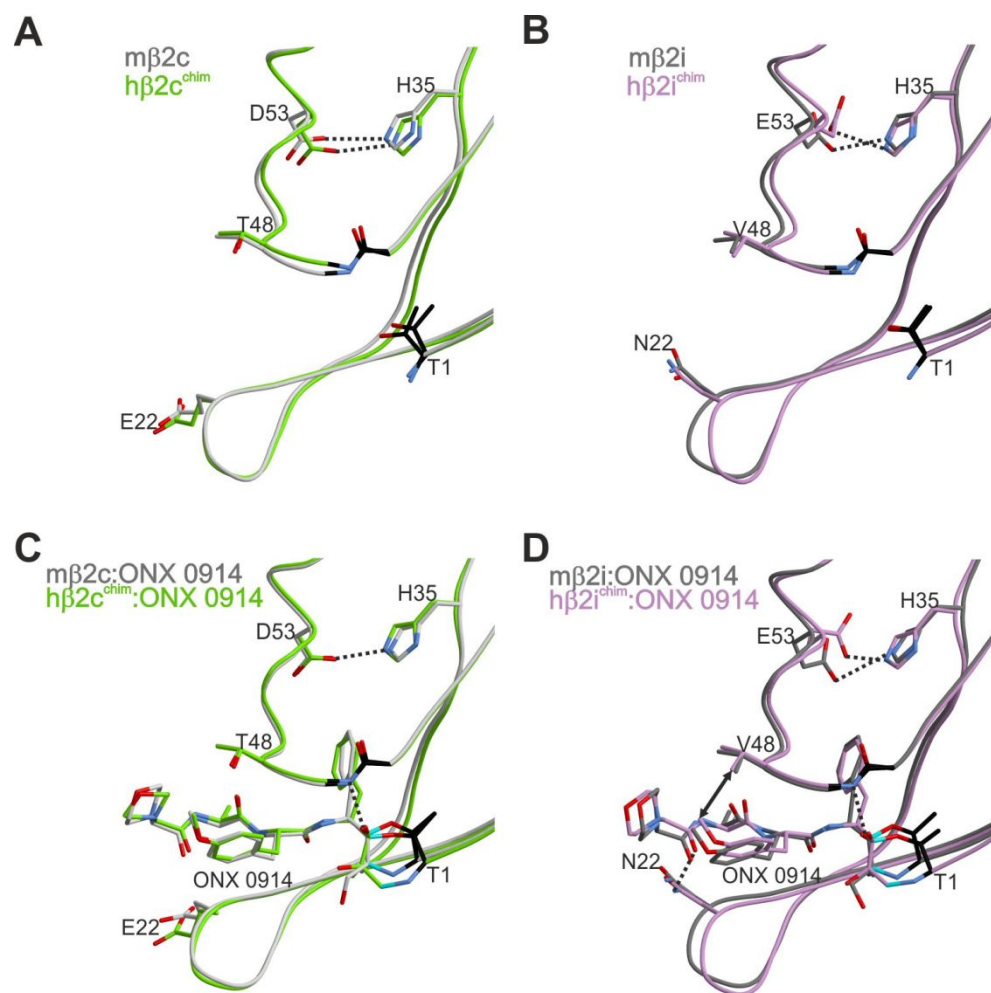


**Figure 5.** Schematic representation of yeast (y) and human (h)  $\beta 2$  subunits and their propeptides. Secondary structure elements, helices (H) and sheets (S) are numbered. (A) The full-length h $\beta 2c$  (green) and h $\beta 2i$  (pink) subunits cannot substitute the endogenous y $\beta 2$  subunit (gray), neither with their natural propeptides (pp; colored) nor with the y $\beta 2$  one (gray) (for details see experimental procedures). Strikingly, the human  $\beta 2c$  subunit can replace the yeast counterpart when featuring the single point mutation S171G<sup>19</sup>. (B) Schematic illustration of human-yeast chimeric  $\beta 2i$  constructs according to panel (A). Sequences highlighted in pink were taken from human  $\beta 2i$ , whereas gray ones originate from the yeast  $\beta 2$  entity. All tested variants, except for the construct encoding the residues 1-53 from human  $\beta 2i$ , caused lethality when expressed in a *pup1* $\Delta$  yeast strain.

Superposition of ligand-free  $\beta 2c/i$  chimeric structures with the natural mouse counterpart<sup>13d</sup> proved their structural similarity (Figure 6A, B). Subsequent crystal soakings with ONX 0914 as a reference compound confirmed that the  $\beta 2$  proteolytic centers were reactive (Figure S9) and visualized a similar binding mode for the inhibitor as in the respective mouse crystal structures<sup>13d</sup> (Figure 6C, D).  $\beta 2$  subunits can accommodate bulky P1 residues without any pronounced

1  
2  
3 conformational changes of the protein backbone (Figure S10A, B). The corresponding spacious  
4 P1 binding site is created by Gly45 at the bottom of the S1 pocket<sup>13d</sup>. While the chemical nature  
5  
6 and the orientation of amino acid 45 differs between most proteasome subunits, Gly45 has been  
7  
8 preserved in  $\beta$ 2 subunits throughout evolution<sup>13d</sup>. Though mutation of Gly45 to Ala does neither  
9  
10 impair yeast growth nor affect subunit folding and ligand binding, any additional increase of  
11  
12 residue 45 is predicted to sterically interfere with the surrounding protein side chains (Figures S8,  
13  
14  
15  
16  
17 S11, S12, Table S13).

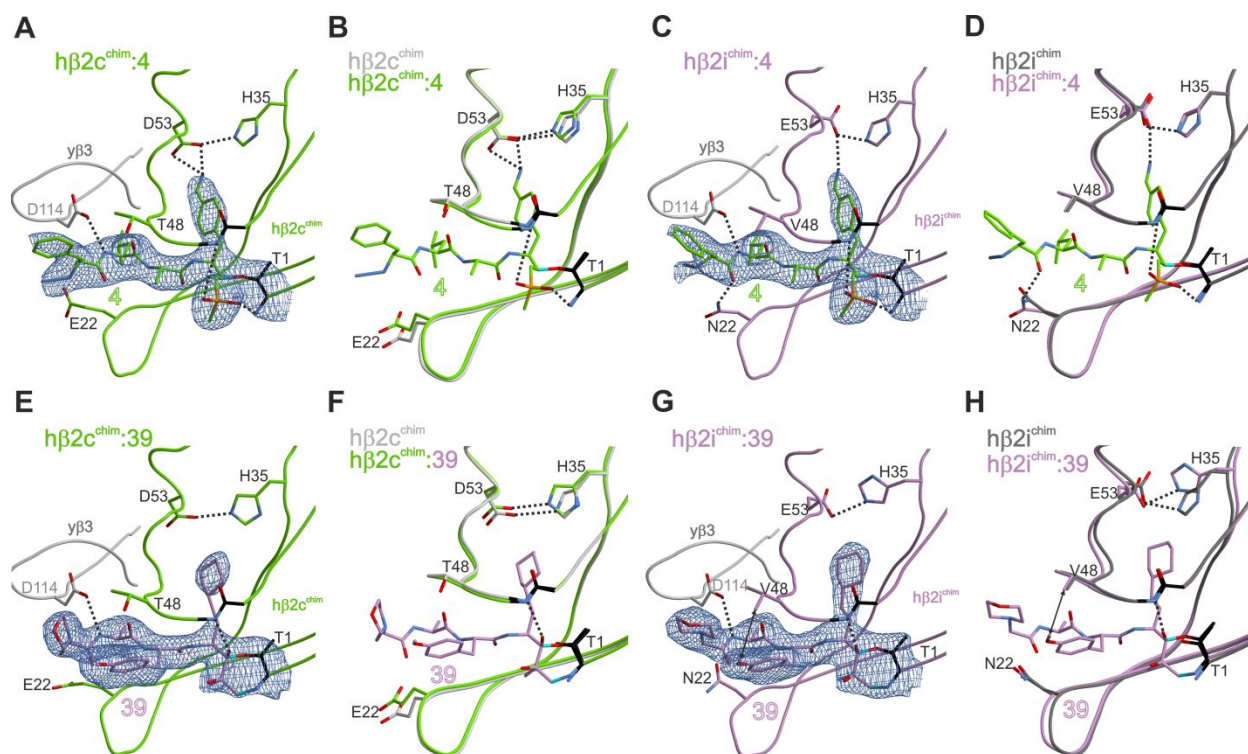
18  
19 Based on the structural similarity of human-yeast chimeric and mouse  $\beta$ 2 active sites, a set of 29  
20  
21 ligand complex structures was determined with WT and  $\beta$ 2 chimeric yeast proteasomes (Table  
22  
23  
24  
25  
26  
27  
28  
29  
30  
31  
32  
33  
34  
35  
36  
37  
38  
39  
40  
41  
42  
43  
44  
45  
46  
47  
48  
49  
50  
51  
52  
53  
54  
55  
56  
57  
58  
59  
60  
S13).



**Figure 6.** Structural superpositions of the natural mouse  $\beta 2c$  (A, C) and  $\beta 2i$  (B, D) subunits with their human-yeast chimeric counterparts in the ligand-free (A, B) and ONX 0914 bound (C, D) states. Amino acids are labelled by the one-letter code. Hydrogen bonds are depicted as black dashed lines. Hydrophobic interactions are highlighted by double arrows. Color coding is according to Figure 5. Note that ONX 0914 has been previously modelled into the mouse  $\beta 2$  subunits as a morpholine adduct with Thr1<sup>13d</sup>, while in the chimeric subunits it was built as a seven-membered ring structure according to the revised reaction mechanism of epoxyketones with Thr1.<sup>21</sup> PDB IDs: 3UNE (mouse cCP), 3UNH (mouse iCP), 3UNB (mouse cCP:ONX 0914),

3UNF (mouse iCP:ONX 0914), 6HTB (h $\beta$ 2c chimera), 6HV3 (h $\beta$ 2i chimera), 6HTC (h $\beta$ 2c chimera:ONX 0914), 6HV4 (h $\beta$ 2i chimera:ONX 0914).

The  $\beta$ 2c-selective compound **4** (LU-002c) was found to be well stabilized in the  $\beta$ 2c and  $\beta$ 2i active sites. Interactions of the 4-aminomethylphenyl group at P1 with the carboxylic amino acid side chains in position 53 are supposed to be the driving force for the general  $\beta$ 2-selectivity of **4** (LU-002c) as well as the related compounds LU-102 (**1**) and LU-112 (**2**) (Figure 1)<sup>16</sup>. Selectivity for subunit  $\beta$ 2c might be gained by dual anchoring of the 4-aminomethylphenyl group to Asp53 in  $\beta$ 2c versus a single interaction with Glu53 in  $\beta$ 2i (Figure 7A, C). In addition, the shorter P2 Ala side chain of **4** (LU-002c) compared to Leu in LU-102 increases  $\beta$ 2c-selectivity by reducing the potency for  $\beta$ 2i (Figure 1). Most likely small P2 residues like Ala fail to undergo favorable van der Waals interactions with Val48 in  $\beta$ 2i (Figure 7C) and thereby lead to the observed  $\beta$ 2c-selectivity of **4** (LU-002c).



**Figure 7.** Human-yeast chimeric proteasomes in complex with  $\beta$ 2c- (**4**; green) and  $\beta$ 2i- (**39**; purple) selective inhibitors. (A, C, E, G)  $2F_O-F_C$  electron density maps for the compounds bound to the  $\beta$ 2c (green) and  $\beta$ 2i (purple) chimeric subunits, respectively, are shown as blue meshes contoured to  $1\sigma$ . (B, D, F, H) Structural superposition of ligand-free and ligand-bound chimeric  $\beta$ 2c and  $\beta$ 2i subunits respectively. Polar and hydrophobic interactions are depicted according to Figure 6. PDB IDs: 6HTB (h $\beta$ 2c chimera), 6HTD (h $\beta$ 2c chimera:**4**), 6HUV (h $\beta$ 2c chimera:**39**), 6HV3 (h $\beta$ 2i chimera), 6HV5 (h $\beta$ 2c chimera:**4**), 6HVV (h $\beta$ 2i chimera:**39**).

For the most selective  $\beta$ 2i-inhibitor, compound **5** (LU-002i), crystallographic data could only be obtained with WT yCP (Figure S13, Table S14). We assume that the ligand could not be trapped at the mutant  $\beta$ 2 active site, since the reactivity of chimeric subunits is impaired<sup>18</sup>, and because compound **5** is poorly soluble in aqueous solutions due to its apolar decaline moiety. Chimeric proteasome structures in complex with **39** however could be achieved. **5** (LU-002i) and **39** are derived from the epoxyketone inhibitor ONX 0914. Epoxyketones have recently been shown to form seven-membered<sup>21</sup> instead of six-membered<sup>22</sup> ring structures with the nucleophilic Thr1 residue of proteasomal  $\beta$  subunits. Although the 1,4-oxazepane (seven-membered) ring structure fits our experimental electron densities in most cases, we also have structural data which matches better the six-membered 1,4-morpholine system (for example see Figure S13A, B). However, the kind of irreversible covalent structure inhibitors form with Thr1 has no further implications for drug development, as subunit selectivity of epoxyketone inhibitors is mostly gained by interactions of the ligands' side chains with the protein surroundings.

ONX 0914 slightly favors  $\beta$ 2i over  $\beta$ 2c<sup>12</sup>, which may be supported by an advantageous hydrophobic interaction of its P2-methoxy group with Val48 of  $\beta$ 2i, a contact that is not provided in subunit  $\beta$ 2c (Figure 6C, D). Furthermore, Asn22 hydrogen bonds to the amide

oxygen atom of the morpholine cap of ONX 0914, while Glu22 in subunit  $\beta 2c$  fails to provide this additional stabilization (Figure 6C, D). The interaction with Asn22 in  $\beta 2i$  is also observed with other tripeptide ligands like **39** (Figure 7G, H), implying that peptide substrates in general might be better stabilized in the  $\beta 2i$  substrate binding channel than in the  $\beta 2c$  one. Notably, a similar observation has previously been reported for Thr22 in subunit  $\gamma \beta 1/\beta 1c^{13a}$ .

The co-crystal structure of the  $\beta 2i$  chimera with compound **39** shows a well-defined  $2F_o - F_c$  electron density map for the ligand (Figure 7G). Comparison of ligand-free and ligand-bound states of the  $\beta 2i$  chimera indicates a movement of His35 upon inhibitor binding (Figure 7H). Despite this structural flexibility and plasticity of the S1 pocket, the hydrogen bond between His35 and Glu53 remains intact. Compared to  $\beta 2i$ , the  $\beta 2c$  active site appears to be more rigid, as binding of **39** does not trigger any structural changes of His35 (Figure 7F). Presumably, the P1 side chain of **39** is less well defined in the  $\beta 2c$  active site due to the tight anchoring of and the resulting steric hindrance with His35 (Figure 7E, F). Thus, although  $\beta 2$  subunits in general accept large P1 side chains, it appears that the plasticity of the  $\beta 2i$  active site tolerates bulky residues even more readily than  $\beta 2c$ .

## Discussion

Here we describe the development and evaluation of a set of potent and selective inhibitors of human  $\beta 2c$  and  $\beta 2i$  proteasome activities. Due to the structural similarities of mammalian  $\beta 2c$  and  $\beta 2i$  subunits, no key guidelines for compound design strategies could be derived from crystal structures so far<sup>13d</sup>. Thus, we used the previously described inhibitors LU-102 (**1**)<sup>16</sup>, LU-112 (**2**)<sup>16</sup> and ONX 0914 (**3**)<sup>12</sup> as starting points, which have no or only moderate preference for one of the two human  $\beta 2$  subunits over the other. By changing the P sites of the ligands we disfavored the most closely related subunit, either  $\beta 2i$  or  $\beta 2c$ , and gained selectivity.

Substantial organic synthesis efforts and thorough empiric screening of compound libraries derived from these lead structures finally led to the identification of selective compounds and to the development of suitable probes for ABPP assays. Furthermore, previously unaddressed stereochemistry issues on LU-002i (**5**) have now been resolved and the exact configuration of the bioactive compound has been determined.

Selected  $\beta$ 2c and  $\beta$ 2i inhibitors were analyzed by X-ray crystallography in complex with the WT yeast CP and with chimeric human-yeast proteasomes, incorporating key elements of the human  $\beta$ 2c and  $\beta$ 2i substrate binding channel, respectively. Despite the artificial character of chimeras they were previously shown to serve as excellent structural tools<sup>18</sup> and now again prove valuable for explaining the selectivity patterns observed for the here described  $\beta$ 2 compound libraries. Both  $\beta$ 2c and  $\beta$ 2i can incorporate large P1 residues in their spacious S1 pocket. Due to favorable hydrogen bond interactions with Asp/Glu53, LU-102 derivatives with their 4-aminomethylphenyl side chain at P1 are in general more potent  $\beta$ 2 inhibitors than ONX 0914-based compounds, featuring apolar P1 residues<sup>16</sup>. Selectivity for  $\beta$ 2c was gained by installing small P2 residues on LU-102. Epoxyketones with bulky hydrophobic P1 residues and small P3 side chains were found to show  $\beta$ 2i-selectivity. Because of the plasticity of the S1 pocket and the flexibility of His35 in subunit  $\beta$ 2i, large apolar P1 side chains can be better accommodated in  $\beta$ 2i than in  $\beta$ 2c.

Taken together, we here present the most selective  $\beta$ 2c and  $\beta$ 2i ligands reported so far. As part of a set of inhibitors and ABPs that is capable of disabling and visualizing the individual activities of human constitutive and immunoproteasomes<sup>15</sup>, these compounds might become valuable tools for fundamental as well as applied biochemical and biomedical research on proteasomes and



hopefully elucidate more details on the biological role and impact of the trypsin-like active sites of human proteasomes.

## Experimental Section

### General procedures

All reagents were of commercial grade and used as received unless indicate otherwise. The purity of all tested compounds is >95% on the basis of LC-MS and NMR. <sup>1</sup>H- and <sup>13</sup>C NMR spectra were recorded on a Bruker AV-400 (400 MHz), AV-600 (600 MHz) or AV-850 (850 MHz) spectrometer. Chemical shifts are given in ppm (δ) relative to CD<sub>3</sub>OD or CDCl<sub>3</sub> as internal standard. Coupling constants are given in Hz and peak assignments are based on 2D <sup>1</sup>H COSY and <sup>13</sup>C HSQC NMR experiments. All <sup>13</sup>C APT spectra are proton decoupled. LC-MS analysis was performed on a Finnigan Surveyor HPLC system with a Gemini C18 50 × 4.60 mm column (detection at 200–600 nm) coupled to a Finnigan LCQ Advantage Max mass spectrometer with ESI. Methods used are: 15 min (0-0.5 min: 10% MeCN; 0.5-10.5 min: 10% to 90% MeCN; 10.5-12.5 min: 90% MeCN; 12.5-15 min: 90% to 10% MeCN) or 12.5 min (0-0.5 min: 10% MeCN; 0.5-8.5 min: 10% to 90% MeCN; 8.5-10.5 min: 90% MeCN; 10.5-12.5 min: 90% to 10% MeCN). HRMS was recorded on a LTQ Orbitrap (ThermoFinnigan). For reverse phase HPLC purification, an automated Gilson HPLC system equipped with a C18 semiprep column (Phenomenex Gemini C18, 5μm 250×10 mm) and a GX281 fraction collector was used.

### General procedure for Boc removal

The appropriate Boc-protected C-terminally modified leucine derivative was dissolved in TFA and stirred for 20 min. Co-evaporation with toluene (3x) afforded the TFA-salt, which was used without further purification.

### General procedure for azide couplings

Compounds **6-53**, **68**, **71**, **74**, **77**, **86**, **87** and **97** were prepared via azide coupling of the appropriate protected tripeptide hydrazide and either an epoxyketone amine or a vinyl sulfone amines. Peptide hydrazides were prepared by hydrazinolysis of peptide methyl esters synthesized as described in the Supporting Information. The hydrazide was dissolved in 1:1 DMF:DCM (v/v) and cooled to -30 °C. *t*BuONO (1.1 eq.) and HCl (4N solution in 1,4-dioxane, 2.8 eq.) were added and the mixture was stirred for 3 h at -30 °C after which TLC analysis (10% MeOH/DCM, v/v) showed complete consumption of the starting material. The epoxyketone or vinyl sulfone amine was added as a free amine to the reaction mixture as a solution in DMF with 5.0 eq. of DiPEA. The mixture was allowed to warm to r.t. overnight. The mixture was diluted with EtOAc and extracted with H<sub>2</sub>O (3x) and brine. The organic layer was dried over MgSO<sub>4</sub> and purified by reverse phase HPLC. For compounds featuring Boc protecting groups, TFA was added and the reaction mixture was stirred for 30 min. The crude was purified by reverse phase HPLC.

N<sub>3</sub>Phe-Leu-Ser-Phe(4-CH<sub>2</sub>NH<sub>2</sub>)VS TFA salt (**13**). The synthesis of tripeptide hydrazide N<sub>3</sub>Phe-Leu-Ser(*t*Bu)-NHNH<sub>2</sub> is described in the Supporting Information. The title compound was prepared according to the general procedure for azide coupling on a 50 μmol scale and purified by HPLC (30%-40% MeCN-H<sub>2</sub>O) to yield 2.8 mg (3.8 μmol, 8%). <sup>1</sup>H NMR (600 MHz, MeOD) δ 7.46-7.23 (m, 9H), 6.85-6.81 (m, 1H), 6.76-6.73 (m, 1H), 4.39-4.27 (m, 2H), 4.20-4.17 (m, 1H), 4.11 (s, 2H), 3.84-3.81 (m, 1H), 3.76-3.73 (m, 1H), 3.25-3.22 (m, 1H), 3.07-2.98 (m, 3H), 2.95 (s, 3H), 1.69-1.52 (m, 3H), 1.02-0.88 (m, 6H). <sup>13</sup>C NMR (150 MHz, MeOD) δ 174.33, 172.23, 171.81, 146.65, 139.69, 137.84, 133.00, 131.84, 131.26, 130.42, 130.24, 129.65, 128.10, 65.38, 62.75, 56.70, 53.80, 52.56, 44.09, 42.77, 41.38, 40.25, 38.72, 25.82, 23.46, 21.84. LC-MS (linear gradient 10 → 90% MeCN/H<sub>2</sub>O, 0.1% TFA, 15.0 min): Rt (min): 6.27 (ESI-MS (m/z): 628.20, (M+H<sup>+</sup>)). HRMS calculated for C<sub>30</sub>H<sub>41</sub>N<sub>7</sub>O<sub>6</sub>S 628.29118 [M+H]<sup>+</sup>; found 628.29123.

Morp-Ala-Tyr(Me)-HomoCha-EK TFA salt (**39**). The synthesis of Boc-HomoCha-EK is described in the Supporting Information and the Boc protecting group was removed according to the general procedure. The title compound was prepared according to the general procedure for azide coupling on a 50  $\mu\text{mol}$  scale and purified by HPLC (30%-45% MeCN-H<sub>2</sub>O) to yield 12.3 mg (17.2  $\mu\text{mol}$ , 34%). <sup>1</sup>H NMR (600 MHz, MeOD)  $\delta$  7.25-7.01 (m, 2H), 6.91-6.67 (m, 2H), 4.60-4.57 (m, 1H), 4.48-4.28 (m, 2H), 3.77 (s, 3H), 3.71-3.70 (m, 4H), 3.21 (d,  $J$  = 4.9 Hz, 1H), 3.09-2.88 (m, 4H), 2.84-2.79 (m, 1H), 2.56-2.37 (m, 4H), 1.83-1.63 (m, 6H), 1.52-1.39 (m, 4H), 1.38-1.16 (m, 9H), 0.97-0.83 (m, 2H). <sup>13</sup>C NMR (150 MHz, MeOD)  $\delta$  209.19, 174.20, 173.30, 171.99, 159.94, 131.41, 130.02, 114.75, 67.85, 62.40, 60.01, 55.75, 55.60, 54.71, 53.06, 52.92, 49.65, 38.48, 38.15, 34.61, 34.02, 29.11, 27.72, 27.44, 27.38, 18.65, 16.84. LC-MS (linear gradient 10  $\rightarrow$  90% MeCN/H<sub>2</sub>O, 0.1% TFA, 12.5 min): Rt (min): 6.23 (ESI-MS ( $m/z$ ): 601.33, ( $M+H^+$ )). HRMS calculated for C<sub>32</sub>H<sub>48</sub>N<sub>4</sub>O<sub>7</sub> 601.35958 [ $M+H$ ]<sup>+</sup>; found 601.35945.

Morp-Ala-Tyr(Me)-1-(*R*)-TetraNal-EK TFA salt (**68**). The synthesis of Boc-1-TetraNal-EK is described in the Supporting Information and the Boc protecting group was removed according to the general procedure. The title compound was prepared according to the general procedure for azide coupling on a 56  $\mu\text{mol}$  scale and purified by HPLC (30%-45% MeCN-H<sub>2</sub>O) to yield 14.2 mg (22.4  $\mu\text{mol}$ , 40%). <sup>1</sup>H NMR (400 MHz, MeOD)  $\delta$  7.22-7.13 (m, 2H), 7.12-7.01 (m, 4H), 6.88-6.77 (m, 2H), 4.63-4.59 (m, 2H), 4.41-4.36 (m, 1H), 4.06-3.84 (m, 6H), 3.78 (s, 3H), 3.17-2.98 (m, 2H), 2.93-2.67 (m, 5H), 2.14-1.54 (m, 6H), 1.45 (s, 3H), 1.35 (d,  $J$  = 7.1 Hz, 3H). <sup>13</sup>C NMR (100 MHz, MeOD)  $\delta$  209.40, 174.19, 173.10, 165.04, 160.01, 140.66, 137.91, 131.40, 130.18, 129.98, 129.94, 127.07, 126.54, 114.84, 64.84, 59.89, 58.37, 55.83, 55.67, 53.93, 52.88, 51.64, 50.57, 39.22, 37.99, 36.17, 30.02, 29.64, 20.16, 18.11, 16.76. LC-MS (linear gradient 10

→ 90% MeCN/H<sub>2</sub>O, 0.1% TFA, 12.5 min): R<sub>t</sub> (min): 6.10 (ESI-MS (m/z): 635.00, (M+H<sup>+</sup>)).

HRMS calculated for C<sub>35</sub>H<sub>46</sub>N<sub>4</sub>O<sub>7</sub> 635.34393 [M+H]<sup>+</sup>; found 635.34371.

Morp-Ala-Tyr(Me)-1-(S)-TetraNal-EK TFA salt (**71**). The synthesis of Boc-1-TetraNal-EK is described in the Supporting Information and the Boc protecting group was removed according to the general procedure. The title compound was prepared according to the general procedure for azide coupling on a 50 μmol scale and purified by HPLC (30%-45% MeCN-H<sub>2</sub>O) to yield 16.5 mg (26.0 μmol, 52%). <sup>1</sup>H NMR (400 MHz, MeOD) δ 7.24-7.13 (m, 3H), 7.13-6.98 (m, 3H), 6.86-6.78 (m, 2H), 4.77-4.59 (m, 2H), 4.41-4.36 (m, 1H), 4.00-3.86 (m, 6H), 3.21 (d, *J* = 5.0 Hz, 1H), 3.10 (dd, *J* = 14.0, 6.0 Hz, 1H), 3.03-2.64 (m, 5H), 2.02-1.60 (m, 6H), 1.45 (s, 3H), 1.33 (d, *J* = 7.2 Hz, 3H). <sup>13</sup>C NMR (100 MHz, MeOD) δ 208.97, 174.18, 173.57, 164.98, 160.01, 141.21, 138.13, 131.41, 130.09, 130.01, 129.75, 126.83, 126.76, 114.84, 114.75, 64.82, 60.04, 58.35, 55.89, 55.66, 53.91, 53.05, 51.05, 50.54, 38.67, 38.02, 35.13, 30.57, 27.13, 20.23, 18.10, 16.86. LC-MS (linear gradient 10 → 90% MeCN/H<sub>2</sub>O, 0.1% TFA, 12.5 min): R<sub>t</sub> (min): 6.18 (ESI-MS (m/z): 635.07, (M+H<sup>+</sup>)). HRMS calculated for C<sub>35</sub>H<sub>46</sub>N<sub>4</sub>O<sub>7</sub> 635.34393 [M+H]<sup>+</sup>; found 635.34370.

Morp-Ala-Tyr(Me)-1-DecAla-EK TFA salt (**74**). The synthesis of Boc-1-DecAla-EK is described in the Supporting Information and the Boc protecting group was removed according to the general procedure. The title compound was prepared according to the general procedure for azide coupling on a 50 μmol scale and purified by HPLC (40%-50% MeCN-H<sub>2</sub>O) to yield 14.6 mg (22.8 μmol, 46%). <sup>1</sup>H NMR (400 MHz, MeOD) δ 7.20-7.11 (m, 2H), 6.86-6.78 (m, 2H), 4.62-4.51 (m, 2H), 4.38-4.33 (m, 1H), 4.07-3.83 (m, 6H), 3.77 (d, *J* = 3.7 Hz, 3H), 3.22 (d, *J* = 12 Hz, 1H), 3.06-3.01 (m, 1H), 2.95 (d, *J* = 12 Hz, 1H), 2.85-2.79 (m, 1H), 1.84-1.13 (m, 25H). <sup>13</sup>C NMR (100 MHz, MeOD) δ 209.81, 174.11, 173.35, 164.81, 159.95, 131.42, 130.00, 114.77,

64.78, 60.08, 58.26, 55.64, 53.89, 52.81, 50.50, 50.29, 39.17, 38.74, 38.20, 33.84, 29.05, 27.91, 26.60, 22.38, 20.22, 18.11, 16.88. LC-MS (linear gradient 10 → 90% MeCN/H<sub>2</sub>O, 0.1% TFA, 12.5 min): R<sub>t</sub> (min): 6.75 (ESI-MS (m/z): 641.13, (M+H<sup>+</sup>)). HRMS calculated for C<sub>35</sub>H<sub>52</sub>N<sub>4</sub>O<sub>7</sub> 641.39088 [M+H]<sup>+</sup>; found 641.39081.

Morp-Ala-Tyr(Me)-1-DecAla-EK TFA salt (**77**). The synthesis of Boc-1-DecAla-EK is described in the Supporting Information and the Boc protecting group was removed according to the general procedure. The title compound was prepared according to the general procedure for azide coupling on a 23 μmol scale and purified by HPLC (40%-50% MeCN-H<sub>2</sub>O) to yield 6.8 mg (10.6 μmol, 46%*s*). <sup>1</sup>H NMR (400 MHz, MeOD) δ 7.19-7.13 (m, 2H), 6.84-6.80 (m, 2H), 4.63-4.60 (m, 1H), 4.53-4.50 (m, 1H), 4.40-4.34 (m, 1H), 4.01-3.90 (m, 6H), 3.78 (d, *J* = 1.9 Hz, 3H), 3.17 (d, *J* = 5.1 Hz, 1H), 3.07-3.02 (m, 1H), 2.94 (d, *J* = 5.1 Hz, 1H), 2.88-2.80 (m, 1H), 1.85-1.07 (m, 25H). <sup>13</sup>C NMR (100 MHz, MeOD) δ 209.46, 174.13, 173.41, 164.82, 159.97, 131.43, 129.96, 114.77, 64.78, 59.91, 58.27, 55.62, 53.90, 52.92, 50.97, 50.52, 43.08, 39.49, 39.11, 38.25, 36.48, 33.73, 27.99, 27.69, 26.76, 26.54, 22.32, 21.21, 18.10, 16.87. LC-MS (linear gradient 10 → 90% MeCN/H<sub>2</sub>O, 0.1% TFA, 12.5 min): R<sub>t</sub> (min): 6.79 (ESI-MS (m/z): 641.07, (M+H<sup>+</sup>)). HRMS calculated for C<sub>35</sub>H<sub>52</sub>N<sub>4</sub>O<sub>7</sub> 641.39088 [M+H]<sup>+</sup>; found 641.39070.

Morp-Ala-Tyr(Me)-1-DecAla-EK TFA salt (**86**). The synthesis of Boc-1-DecAla-EK is described in the Supporting Information and the Boc protecting group was removed according to the general procedure. The title compound was prepared according to the general procedure for azide coupling on a 25 μmol scale and purified by HPLC (30%-45% MeCN-H<sub>2</sub>O) to yield 8.6 mg (11.4 μmol, 46%). <sup>1</sup>H NMR (500 MHz, MeOD) δ 7.15 (d, *J* = 8.7 Hz, 2H), 6.85-6.80 (m, 2H), 4.62-4.59 (m, 1H), 4.55-4.52 (m, 1H), 4.40-4.35 (m, 1H), 4.01-3.91 (m, 6H), 3.78 (s, 3H), 3.21 (d, *J* = 5.1 Hz, 1H), 3.07-3.03 (m, 1H), 2.95 (d, *J* = 5.1 Hz, 1H), 2.85-2.81 (m, 1H), 1.83-

1.52 (m, 10H), 1.47-1.41 (m, 5H), 1.37-1.18 (m, 10H).  $^{13}\text{C}$  NMR (125 MHz, MeOD)  $\delta$  209.83, 174.13, 173.36, 164.80, 159.96, 131.42, 129.99, 114.77, 64.78, 60.09, 58.26, 55.64, 53.90, 52.81, 50.49, 50.29, 39.21, 39.17, 38.75, 38.20, 34.85, 33.84, 29.05, 27.92, 27.91, 26.60, 22.38, 20.22, 18.12, 16.87. LC-MS (linear gradient 10  $\rightarrow$  90% MeCN/H<sub>2</sub>O, 0.1% TFA, 12.5 min):  $R_t$  (min): 6.92 (ESI-MS (m/z): 641.13, (M+H<sup>+</sup>)). HRMS calculated for C<sub>35</sub>H<sub>52</sub>N<sub>4</sub>O<sub>7</sub> 641.39088 [M+H]<sup>+</sup>; found 641.39065.

Morp-Ala-Tyr(Me)-1-DecAla-EK TFA salt (**87**). The synthesis of Boc-1-DecAla-EK is described in the Supporting Information and the Boc protecting group was removed according to the general procedure. The title compound was prepared according to the general procedure for azide coupling on a 44  $\mu\text{mol}$  scale and purified by HPLC (30%-45% MeCN-H<sub>2</sub>O) to yield 12.7 mg (16.8  $\mu\text{mol}$ , 38%).  $^1\text{H}$  NMR (500 MHz, MeOD)  $\delta$  7.15 (d,  $J$  = 8.6 Hz, 2H), 6.84-6.79 (m, 2H), 4.66-4.58 (m, 1H), 4.53-4.50 (m, 1H), 4.39-4.35 (m, 1H), 4.02-3.92 (m, 6H), 3.17 (d,  $J$  = 5.1 Hz, 1H), 3.07-3.03 (m, 1H), 2.94 (d,  $J$  = 5.1 Hz, 1H), 2.86-2.82 (m, 1H), 1.84-1.18 (m, 25H).  $^{13}\text{C}$  NMR (125 MHz, MeOD)  $\delta$  209.47, 174.13, 173.41, 164.81, 159.96, 131.43, 129.96, 114.77, 64.76, 59.91, 58.24, 55.64, 53.89, 52.93, 50.96, 50.55, 43.06, 39.48, 39.10, 38.25, 36.48, 33.72, 27.98, 27.68, 26.75, 26.53, 22.31, 21.21, 18.08, 16.87. LC-MS (linear gradient 10  $\rightarrow$  90% MeCN/H<sub>2</sub>O, 0.1% TFA, 12.5 min):  $R_t$  (min): 6.88 (ESI-MS (m/z): 641.13, (M+H<sup>+</sup>)). HRMS calculated for C<sub>35</sub>H<sub>52</sub>N<sub>4</sub>O<sub>7</sub> 641.39088 [M+H]<sup>+</sup>; found 641.39077.

Morp-Ala-Tyr(O-C<sub>2</sub>H<sub>4</sub>-BODIPY(FL))-1-DecAla-EK (**97**). The synthesis of compound **95** is described in the Supporting Information. Compound **95** (23 mg, 33  $\mu\text{mol}$ ) and BODIPY-FL-alkyne **96**<sup>23</sup> (13 mg, 40  $\mu\text{mol}$ , 1.2 eq.) were dissolved in DMF. An aqueous solution of sodium ascorbate (100  $\mu\text{L}$ , 25  $\mu\text{mol}$ , 0.75 eq.) and an aqueous solution of CuSO<sub>4</sub> (100  $\mu\text{L}$ , 17  $\mu\text{mol}$ , 0.5 eq.) were added. The reaction mixture was stirred at r.t. overnight. The reaction mixture was

concentrated in vacuo and purification by HPLC (50-70% MeCN-H<sub>2</sub>O) yielded the title compound (6.7 mg, 5.9  $\mu$ mol, 18%). <sup>1</sup>H NMR (600 MHz, MeOD)  $\delta$  7.91 (s, 1H), 7.17 (d, J = 8.2 Hz, 2H), 6.84 (dd, J = 12.1, 8.3 Hz, 2H), 6.14 (s, 2H), 4.82 (t, J = 5.0 Hz, 2H), 4.64 (dt, J = 8.3, 5.5 Hz, 1H), 4.57 (ddd, J = 13.6, 10.7, 3.3 Hz, 1H), 4.46-4.34 (m, 4H), 3.99 (dd, J = 24.6, 16.0 Hz, 8H), 3.34-3.16 (m, 3H), 3.16-3.03 (m, 4H), 2.98 (dt, J = 11.4, 5.6 Hz, 1H), 2.87 (t, J = 7.2 Hz, 4H), 2.51 (s, 8H), 2.44 (s, 8H), 1.99 (q, J = 7.4 Hz, 3H), 1.93-1.80 (m, 3H), 1.75 (ddd, J = 16.6, 8.4, 3.4 Hz, 6H), 1.69-1.54 (m, 6H), 1.52 (d, J = 2.8 Hz, 1H), 1.49 (d, J = 2.9 Hz, 5H), 1.45-1.37 (m, 5H), 1.37-1.18 (m, 7H). <sup>13</sup>C NMR (150 MHz, MeOD)  $\delta$  209.76, 209.41, 174.09, 173.28, 173.22, 172.91, 164.76, 161.88, 161.64, 158.47, 154.93, 148.55, 147.84, 142.18, 132.57, 131.57, 130.91, 130.89, 130.77, 124.23, 122.62, 115.63, 115.58, 67.69, 64.80, 64.75, 60.04, 59.87, 58.23, 55.64, 53.89, 52.90, 52.77, 50.96, 50.52, 50.20, 49.43, 49.28, 49.14, 49.00, 48.86, 48.72, 48.57, 43.06, 39.48, 39.22, 39.11, 38.74, 38.28, 38.23, 36.50, 35.66, 34.99, 34.89, 33.84, 33.73, 32.20, 32.15, 30.72, 30.63, 29.08, 29.04, 27.99, 27.91, 27.69, 27.58, 27.00, 26.76, 26.59, 26.53, 25.88, 22.38, 22.31, 21.21, 18.14, 16.88, 16.49, 14.48. LC-MS (linear gradient 10  $\rightarrow$  90% MeCN/H<sub>2</sub>O, 0.1% TFA, 12.5 min): Rt (min): 8.07 (ESI-MS (m/z): 1024.33, (M+H<sup>+</sup>)). HRMS calculated for C<sub>55</sub>H<sub>78</sub>BF<sub>2</sub>N<sub>9</sub>O<sub>7</sub> 1024.60108 [M+H]<sup>+</sup>; found 1024.60174.

### Biological and Structural Analysis.

**Competition Assays in Cell Lysates.** Lysates of Raji cells were prepared by sonication in 3 volumes of lysis buffer containing 50 mM Tris pH 7.5, 1 mM DTT, 5 mM MgCl<sub>2</sub>, 250 mM sucrose, 2 mM ATP, and 0.05% (w/v) digitonin. Protein concentration was determined by the Bradford assay. Cell lysates (diluted to 5  $\mu$ g of total protein in buffer containing 50 mM Tris pH 7.5, 2 mM DTT, 5 mM MgCl<sub>2</sub>, 10% (v/v) glycerol, 2 mM ATP) were exposed to the inhibitors for 1 h at 37  $^{\circ}$ C prior to incubation with cocktail ABPs for another 1 h, followed by 3 min

boiling with a reducing gel-loading buffer and fractionation on 12.5% SDS PAGE. In-gel detection of residual proteasome activity was performed in the wet gel slabs directly on a ChemiDoc™ MP system using Cy2 settings to detect BODIPY(FL)-LU-112, Cy3 settings to detect BODIPY(TMR)-NC-005-VS and Cy5 settings to detect Cy5-NC-001. Intensities of bands were measured by fluorescent densitometry and normalized to the intensity of bands in mock-treated extracts. Average values of three independent experiments were plotted against inhibitor concentrations (In the initial screening, experiments were only carried out one time). IC<sub>50</sub> (ligand concentrations giving 50% inhibition) values were calculated using GraphPad Prism software.

**Competition Assays in living RPMI-8226 cells.** RPMI-8226 were cultured in RPMI-1640 media supplemented with 10% (v/v) fetal calf serum, GlutaMAX™, penicillin/streptomycin in a 5% CO<sub>2</sub> humidified incubator. An amount of (5-8) x10<sup>5</sup> cells/mL cells was exposed to inhibitors for 1 h at 37 °C. Cells were harvested and washed twice with PBS. Cell pellets were treated with lysis buffer (50 mM Tris pH 7.5, 2 mM DTT, 5 mM MgCl<sub>2</sub>, 10% (v/v) glycerol, 2 mM ATP, 0.05% (w/v) digitonin) on ice for 1 h, followed by centrifugation at 14000 rpm for 15 min. Proteasome inhibition in the obtained cell lysates was determined using the method described above. Intensities of bands were measured by fluorescent densitometry and divided by the intensity of bands in mock-treated extracts. Gels were stained by Coomassie Brilliant Blue, which was used to correct for gel loading differences. Average values of three independent experiments were plotted against inhibitor concentrations. IC<sub>50</sub> (compound concentrations causing 50% inhibition) values were calculated using GraphPad Prism software.

**Activity-Based Protein Profiling Assays in Raji Cell Lysates.** Raji cell lysates (diluted to 5 µg of total protein in buffer containing 50 mM Tris pH 7.5, 2 mM DTT, 5 mM MgCl<sub>2</sub>, 10% (v/v) glycerol, 2 mM ATP) were exposed to the probe for 1 h at 37 °C prior, followed by 3 min



boiling with a reducing gel-loading buffer and fractionation on 12.5% SDS PAGE. Separation was obtained by electrophoresis for 15 min on 80V, followed by 120 min on 130 V. In-gel detection of residual proteasome activity was performed in the wet gel slabs directly on a ChemiDoc™ MP system using Cy2 settings.

**Yeast mutagenesis.** hPSMB7 and hPSMB10 encoding the human  $\beta 2c$  and  $\beta 2i$  proteasome subunits, respectively, were purchased as yeast codon optimized, synthetic gene fragments each with an 30 bp 5'-overhang corresponding to the yeast *PUP1* promoter sequence preceding the start ATG and an 40 bp 3'-overhang corresponding to the *PUP1* terminator sequence following the stop codon. An AgeI site at the codons for Gly-1/Thr1 was incorporated into both genes.

The human PSMB7/10 ORFs were fused to the *PUP1* promoter and terminator by recombinant PCRs: Both genes were amplified with primers PSMB-for and PSMB-rev (Table S15). The *PUP1* promoter was amplified from template plasmid p15-PUP1-new with primers pBS-rev and PUP1-prom-rev and the terminator with primers PUP1-ter-for and pBS-uni (Table S15). The promoter fragment and the ORF fragments were fused by recombinant PCR in the presence of pBS-rev and PSMB-rev. The resulting fragment was then fused by recombinant PCR with the terminator fragment in the presence of pBS-rev and pBS-uni.

The recombinant gene fragments were cut with SacI and HindIII and ligated with SacI/HindIII cut vector pUC19 and afterwards transferred into shuttle vector pRS315 yielding p15-fl-PSMB7 and p15-fl-PSMB10. The S171G mutant version of PSMB7 was created by recombinant PCR with the pUC19 construct as template and mutagenic primers PSMB7-S171G-for and PSMB7-S171G-rev (Table S15) and cloning of the resulting SacI/HindIII cut product into pRS315 yielding p15-fl-PSMB7\*.

For replacement of the genuine human propeptide encoding sequences by the *PUP1* propeptide sequence the *PUP1* promoter together with the propeptide encoding region were amplified from p15-PUP1<sup>20b</sup> with primers pBS-rev and PUP1-Age-rev (Table S15), which introduces an AgeI site at the corresponding Gly-1/Thr1 encoding position of *PUP1*. The PCR product was cut with HindIII and AgeI and ligated with the respective AgeI/SacI fragments from p15-fl-PSMB7, p15-fl-PSMB7\* and p15-fl-PSMB10 into HindIII/SacI cut pRS315 in order to obtain plasmids p15-P1pp-PSMB7, p15-P1pp-PSMB7\* and p15-P1pp-PSMB10.

Genes encoding hybrids of  $\gamma\beta 2$  and  $h\beta 2i$  were constructed by recombinant PCR. For the  $h\beta 2i^{1-129}$  construct an N-terminal fragment resulting from a PCR with primers pBS-rev and beta2i-129-rev on template p15-P1pp-PSMB10 was fused with a C-terminal fragment made by PCR with primers beta2i-129-for and pBS-uni on template p15-PUP1-new (Table S15). Accordingly, the hybrids  $h\beta 2i^{1-93}$  and  $h\beta 2i^{1-52}$  were constructed employing primers beta2i-1-93-for/ beta2i-1-93-rev and beta2i-1-52-for/ beta2i-1-52-rev, respectively. For the  $h\beta 2i^{1-52/93-129}$  hybrid, the N-terminal fragment was obtained by PCR on the  $h\beta 2i^{1-52}$  template with primers pBS-rev and y93-rev and for the C-terminal fragment the  $h\beta 2i^{1-129}$  template was used with primers 2i93-for and pBS-uni (Table S15).

All pRS315-based constructs were introduced into yeast strain YWH10<sup>20b</sup>, which has the chromosomal *PUP1* gene deleted and a wild-type *PUP1* copy in an *URA3*-marked plasmid. After selection against *URA3* on 5'-fluoruracil clones that were viable without the wild-type *PUP1* gene were recovered.

**Crystallographic analysis.** WT and mutant yCP crystals were grown by hanging drop vapor diffusion as previously described.<sup>24</sup> Inhibitor complex structures were obtained by incubating crystals in 5  $\mu$ l cryobuffer (20 mM magnesium acetate, 100 mM 2-(*N*-morpholino)ethanesulfonic

acid, pH 6.8 and 30% (v/v) 2-methyl-2,4-pentanediol) supplemented with 0.5  $\mu$ l of inhibitor (50 mM in dimethyl sulfoxide) for up to 48 h. Diffraction data were collected at the beamline X06SA at the Paul Scherrer Institute, SLS, Villigen, Switzerland ( $\lambda = 1.0$  Å). Evaluation of reflection intensities and data reduction were performed with the program package XDS.<sup>25</sup> Molecular replacement was carried out with the coordinates of the yeast 20S proteasome (PDB entry code: 5CZ4<sup>26</sup>) by rigid body refinements (REFMAC5<sup>27</sup>). COOT<sup>28</sup> was used to build models. Translation/libration/screw refinements finally yielded excellent R factors as well as r.m.s.d. bond and angle values. The coordinates, proven to have good stereochemistry from the Ramachandran plots, were deposited in the RCSB Protein Data Bank. For accession codes see Table S13.

## ASSOCIATED CONTENT

### Supporting Information

Assays of compounds **6-53** and **68, 71, 74, 77, 86, 87** and **97** in Raji lysates, pIC<sub>50</sub> values and standard errors of all compounds in cell lysates and intact cells, structures of activity-based probes, complete synthetic details and characterization of all compounds and synthetic intermediates, NMR spectra and LC-MS traces of compounds **13, 39, 68, 71, 74, 77, 86, 87**, and **97** as well as X-ray data tables and oligonucleotides. The Molecular Formula String is also available as CSV file. PDB IDs are listed in Table S13. Authors will release the atomic coordinates upon article publication. This material is available free of charge via the internet at <http://pubs.acs.org>.

### Accession Codes

Structure factors and coordinates were deposited in the RCSB Protein Data Bank under the accession codes listed in Table S13.

## AUTHOR INFORMATION

### Corresponding Author

\*Phone: +31- 71-5274342; fax: +31-71-527-4307; e-mail: [h.s.overkleeft@chem.leidenuniv.nl](mailto:h.s.overkleeft@chem.leidenuniv.nl).

\*Phone: +49-89-289-13361; fax: +49-89-289-13361; e-mail: [michael.groll@tum.de](mailto:michael.groll@tum.de)

### Funding Sources

This work was supported by the China Scholarship Council (PhD-fellowship, to B.-T.X.), The Netherlands Organization for Scientific Research (NWO, TOPPUNT grant, to H.S.O.), the Young Scholars' Program of the Bavarian Academy of Sciences and Humanities (fellowship, to E.M.H) and by the Deutsche Forschungsgemeinschaft (DFG, Grant GR1861/10-1 to M.G.).

### Notes

The authors declare no competing financial interest.

## ACKNOWLEDGMENT

We thank the staff of the beamlines X06SA at the Paul Scherrer Institute, Swiss Light Source, Villigen (Switzerland) and ID23 at the European Synchrotron Radiation Facility, Grenoble (France) for assistance during data collection. Richard Feicht is greatly acknowledged for the purification and crystallization of proteasome mutants.

## ABBREVIATIONS

ABPP, activity-based protein profiling; ABP, activity-based probe; BODIPY, boron-dipyrrromethene, (4,4-difluoro-5,7-dimethyl-4-bora-3a,4a-diaza-s-indacene); cCP, constitutive proteasome core particles; iCP, immunoproteasome core particles, DiPEA, *N,N*-

diisopropylethylamine; EtOAc, ethyl acetate; HCTU, 2-(6-chloro-1H-benzotriazol-1-yl)-1,1,3,3-tetramethyluronium hexafluorophosphate.

## REFERENCES

1. (a) Hershko, A.; Ciechanover, A., The ubiquitin system. *Annu. Rev. Biochem.* **1998**, *67*, 425-479; (b) Rock, K. L.; Gramm, C.; Rothstein, L.; Clark, K.; Stein, R.; Dick, L.; Hwang, D.; Goldberg, A. L., Inhibitors of the proteasome block the degradation of most cell proteins and the generation of peptides presented on MHC class I molecules. *Cell* **1994**, *78*, 761-771.
2. (a) Löwe, J.; Stock, D.; Jap, B.; Zwickl, P.; Baumeister, W.; Huber, R., Crystal structure of the 20S proteasome from the archaeon *T. acidophilum* at 3.4 Å resolution. *Science* **1995**, *268*, 533-539; (b) Groll, M.; Ditzel, L.; Löwe, J.; Stock, D.; Bochtler, M.; Bartunik, H. D.; Huber, R., Structure of 20S proteasome from yeast at 2.4 Å resolution. *Nature* **1997**, *386*, 463-471.
3. Voges, D.; Zwickl, P.; Baumeister, W., The 26S proteasome: a molecular machine designed for controlled proteolysis. *Annu. Rev. Biochem.* **1999**, *68*, 1015-1068.
4. (a) Aki, M.; Shimbara, N.; Takashina, M.; Akiyama, K.; Kagawa, S.; Tamura, T.; Tanahashi, N.; Yoshimura, T.; Tanaka, K.; Ichihara, A., Interferon-gamma induces different subunit organizations and functional diversity of proteasomes. *J. Biochem.* **1994**, *115*, 257-269; (b) Griffin, T. A.; Nandi, D.; Cruz, M.; Fehling, H. J.; Kaer, L. V.; Monaco, J. J.; Colbert, R. A., Immunoproteasome assembly: cooperative incorporation of interferon gamma (IFN-gamma)-inducible subunits. *J. Exp. Med.* **1998**, *187*, 97-104; (c) Groettrup, M.; Kraft, R.; Kostka, S.; Standera, S.; Stohwasser, R.; Kloetzel, P. M., A third interferon-gamma-induced subunit exchange in the 20S proteasome. *Eur. J. Immunol.* **1996**, *26*, 863-869.

5. Basler, M.; Kirk, C. J.; Groettrup, M., The immunoproteasome in antigen processing and other immunological functions. *Curr. Opin. Immunol.* **2013**, *25*, 74-80.
6. (a) Huber, E. M.; Groll, M., Inhibitors for the immuno- and constitutive proteasome: current and future trends in drug development. *Angew. Chem. Int. Ed.* **2012**, *51*, 8708-8720; (b) Beck, P.; Dubiella, C.; Groll, M., Covalent and non-covalent reversible proteasome inhibition. *Biol. Chem.* **2012**, *393*, 1101-1120; (c) Kisselev, A. F.; van der Linden, W. A.; Overkleeft, H. S., Proteasome inhibitors: an expanding army attacking a unique target. *Chem. Biol.* **2012**, *19*, 99-115.
7. Borissenko, L.; Groll, M., 20S proteasome and its inhibitors: crystallographic knowledge for drug development. *Chem. Rev.* **2007**, *107*, 687-717.
8. (a) Screen, M.; Britton, M.; Downey, S. L.; Verdoes, M.; Voges, M. J.; Blom, A. E.; Geurink, P. P.; Risseuw, M. D.; Florea, B. I.; van der Linden, W. A.; Pletnev, A. A.; Overkleeft, H. S.; Kisselev, A. F., Nature of pharmacophore influences active site specificity of proteasome inhibitors. *J. Biol. Chem.* **2010**, *285*, 40125-40134; (b) Verdoes, M.; Willems, L. I.; van der Linden, W. A.; Duivenvoorden, B. A.; van der Marel, G. A.; Florea, B. I.; Kisselev, A. F.; Overkleeft, H. S., A panel of subunit-selective activity-based proteasome probes. *Org. Biomol. Chem.* **2010**, *8*, 2719-2727.
9. (a) Fostier, K.; De Becker, A.; Schots, R., Carfilzomib: a novel treatment in relapsed and refractory multiple myeloma. *OncoTargets Ther.* **2012**, *5*, 237-244; (b) Field-Smith, A.; Morgan, G. J.; Davies, F. E., Bortezomib (Velcade™) in the treatment of multiple myeloma. *Ther. Clin. Risk Manag.* **2006**, *2*, 271-279.
10. Vallumsetla, N.; Paludo, J.; Kapoor, P., Bortezomib in mantle cell lymphoma: comparative therapeutic outcomes. *Ther. Clin. Risk Manag.* **2015**, *11*, 1663-1674.

11. Johnson, H. W. B.; Lowe, E.; Anderl, J. L.; Fan, A.; Muchamuel, T.; Bowers, S.; Moebius, D.; Kirk, C.; McMinn, D. L., A required immunoproteasome subunit inhibition profile for anti-inflammatory efficacy and clinical candidate KZR-616 ((2S,3R)-N-((S)-3-(cyclopent-1-en-1-yl)-1-((R)-2-methyloxiran-2-yl)-1-oxopropan-2-yl)-3-hydroxy-3-(4-methoxyphenyl)-2-((S)-2-(2-morpholinoacetamido)propanamido)propenamide). *J. Med. Chem.* **2018**, *61*, 11127-11143.
12. Muchamuel, T.; Basler, M.; Aujay, M. A.; Suzuki, E.; Kalim, K. W.; Lauer, C.; Sylvain, C.; Ring, E. R.; Shields, J.; Jiang, J.; Shwonek, P.; Parlati, F.; Demo, S. D.; Bennett, M. K.; Kirk, C. J.; Groettrup, M., A selective inhibitor of the immunoproteasome subunit LMP7 blocks cytokine production and attenuates progression of experimental arthritis. *Nat. Med.* **2009**, *15*, 781-787.
13. (a) Huber, E. M.; de Bruin, G.; Heinemeyer, W.; Paniagua Soriano, G.; Overkleeft, H. S.; Groll, M., Systematic analyses of substrate preferences of 20S proteasomes using peptidic epoxyketone inhibitors. *J. Am. Chem. Soc.* **2015**, *137*, 7835-7842; (b) de Bruin, G.; Huber, E. M.; Xin, B. T.; van Rooden, E. J.; Al-Ayed, K.; Kim, K. B.; Kisselev, A. F.; Driessen, C.; van der Stelt, M.; van der Marel, G. A.; Groll, M.; Overkleeft, H. S., Structure-based design of beta1i or beta5i specific inhibitors of human immunoproteasomes. *J. Med. Chem.* **2014**, *57*, 6197-6209; (c) Parlati, F.; Lee, S. J.; Aujay, M.; Suzuki, E.; Levitsky, K.; Lorens, J. B.; Micklem, D. R.; Ruurs, P.; Sylvain, C.; Lu, Y.; Shenk, K. D.; Bennett, M. K., Carfilzomib can induce tumor cell death through selective inhibition of the chymotrypsin-like activity of the proteasome. *Blood* **2009**, *114*, 3439-3447; (d) Huber, E. M.; Basler, M.; Schwab, R.; Heinemeyer, W.; Kirk, C. J.; Groettrup, M.; Groll, M., Immuno- and constitutive proteasome crystal structures reveal differences in substrate and inhibitor specificity. *Cell* **2012**, *148*, 727-738; (e) Xin, B. T.; de Bruin, G.; Huber, E. M.; Besse, A.; Florea, B. I.; Filippov, D. V.; van der Marel, G. A.; Kisselev,

- A. F.; van der Stelt, M.; Driessen, C.; Groll, M.; Overkleeft, H. S., Structure-based design of beta5c selective inhibitors of human constitutive proteasomes. *J. Med. Chem.* **2016**, *59*, 7177-7187; (f) Johnson, H. W. B.; Anderl, J. L.; Bradley, E. K.; Bui, J.; Jones, J.; Arastu-Kapur, S.; Kelly, L. M.; Lowe, E.; Moebius, D. C.; Muchamuel, T.; Kirk, C.; Wang, Z.; McMin, D., Discovery of highly selective inhibitors of the immunoproteasome low molecular mass molyptide 2 (LMP2) subunit. *ACS Med. Chem. Lett.* **2017**, *8*, 413-417.
14. Artschwager, R.; Ward, D. J.; Gannon, S.; Brouwer, A. J.; van de Langemheen, H.; Kowalski, H.; Liskamp, R. M. J., Potent and highly selective inhibitors of the proteasome trypsin-like site by incorporation of basic side chain containing amino acid derived sulfonyl fluorides. *J. Med. Chem.* **2018**, *61*, 5395-5411.
15. de Bruin, G.; Xin, B. T.; Kraus, M.; van der Stelt, M.; van der Marel, G. A.; Kisselev, A. F.; Driessen, C.; Florea, B. I.; Overkleeft, H. S., A set of activity-based probes to visualize human (immuno)proteasome activities. *Angew. Chem. Int. Ed.* **2016**, *55*, 4199-4203.
16. Geurink, P. P.; van der Linden, W. A.; Mirabella, A. C.; Gallastegui, N.; de Bruin, G.; Blom, A. E.; Voges, M. J.; Mock, E. D.; Florea, B. I.; van der Marel, G. A.; Driessen, C.; van der Stelt, M.; Groll, M.; Overkleeft, H. S.; Kisselev, A. F., Incorporation of non-natural amino acids improves cell permeability and potency of specific inhibitors of proteasome trypsin-like sites. *J. Med. Chem.* **2013**, *56*, 1262-1275.
17. (a) Mirabella, A. C.; Pletnev, A. A.; Downey, S. L.; Florea, B. I.; Shabaneh, T. B.; Britton, M.; Verdoes, M.; Filippov, D. V.; Overkleeft, H. S.; Kisselev, A. F., Specific cell-permeable inhibitor of proteasome trypsin-like sites selectively sensitizes myeloma cells to bortezomib and carfilzomib. *Chem. Biol.* **2011**, *18*, 608-618; (b) Weyburne, E. S.; Wilkins, O. M.; Sha, Z.; Williams, D. A.; Pletnev, A. A.; de Bruin, G.; Overkleeft, H. S.; Goldberg, A. L.;



Cole, M. D.; Kisselev, A. F., Inhibition of the proteasome beta2 site sensitizes triple-negative breast cancer cells to beta5 inhibitors and suppresses Nrf1 activation. *Cell. Chem. Biol.* **2017**, *24*, 218-230.

18. Huber, E. M.; Heinemeyer, W.; de Bruin, G.; Overkleeft, H. S.; Groll, M., A humanized yeast proteasome identifies unique binding modes of inhibitors for the immunosubunit beta5i. *Embo J.* **2016**, *35*, 2602-2613.

19. Kachroo, A. H.; Laurent, J. M.; Yellman, C. M.; Meyer, A. G.; Wilke, C. O.; Marcotte, E. M., Evolution. Systematic humanization of yeast genes reveals conserved functions and genetic modularity. *Science* **2015**, *348*, 921-925.

20. (a) Groll, M.; Heinemeyer, W.; Jäger, S.; Ullrich, T.; Bochtler, M.; Wolf, D. H.; Huber, R., The catalytic sites of 20S proteasomes and their role in subunit maturation: a mutational and crystallographic study. *Proc. Natl. Acad. Sci. U. S. A.* **1999**, *96*, 10976-10983; (b) Heinemeyer, W.; Fischer, M.; Krimmer, T.; Stachon, U.; Wolf, D. H., The active sites of the eukaryotic 20 S proteasome and their involvement in subunit precursor processing. *J. Biol. Chem.* **1997**, *272*, 25200-25209.

21. Schrader, J.; Henneberg, F.; Mata, R. A.; Tittmann, K.; Schneider, T. R.; Stark, H.; Bourenkov, G.; Chari, A., The inhibition mechanism of human 20S proteasomes enables next-generation inhibitor design. *Science* **2016**, *353* (6299), 594-598.

22. Groll, M.; Kim, K. B.; Kairies, N.; Huber, R.; Crews, C. M., Crystal structure of epoxomicin: 20S proteasome reveals a molecular basis for selectivity of  $\alpha'$ ,  $\beta'$ -epoxyketone proteasome inhibitors. *J. Am. Chem. Soc.* **2000**, *122*, 1237-1238.

23. Verdoes, M.; Hillaert, U.; Florea, B. I.; Sae-Heng, M.; Risseuw, M. D. P.; Filippov, D. V.; van der Marel, G. A.; Overkleeft, H. S., Acetylene functionalized BODIPY dyes and their

1  
2  
3 application in the synthesis of activity based proteasome probes. *Bioorg. Med. Chem. Lett.* **2007**,  
4  
5 *17*, 6169-6171.

6  
7  
8 24. Gallastegui, N.; Groll, M., Analysing properties of proteasome inhibitors using kinetic  
9  
10 and X-ray crystallographic studies. *Methods Mol. Biol.* **2012**, 832, 373-390.

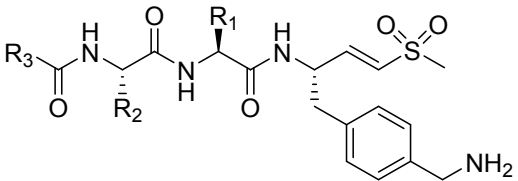
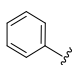
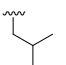
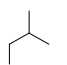
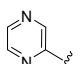
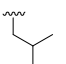
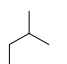
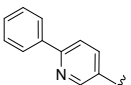
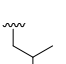
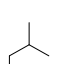
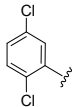
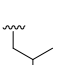
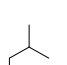
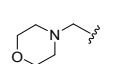
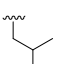
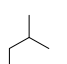
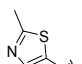
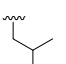
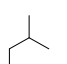
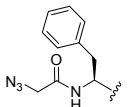
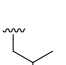
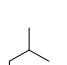
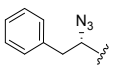
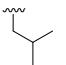
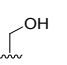
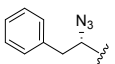
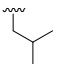
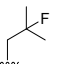
11  
12 25. Kabsch, W., X. D. S. *Acta Crystallogr. Sect. D - Biol. Crystallogr.* **2010**, 66, 125-132.

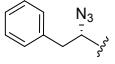
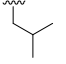
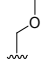
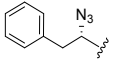
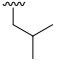

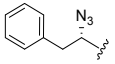
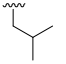
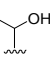
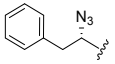
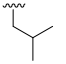
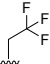
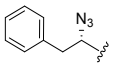
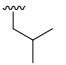
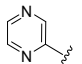
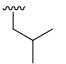

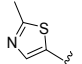
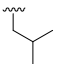
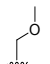
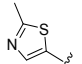
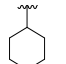
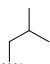
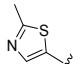
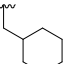
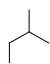
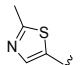
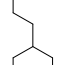
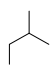
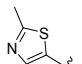
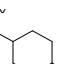
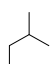
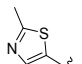
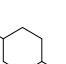
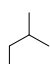
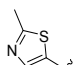
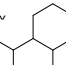
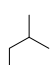
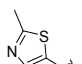
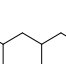
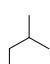
13  
14 26. Huber, E. M.; Heinemeyer, W.; Li, X.; Arendt, C. S.; Hochstrasser, M.; Groll, M., A  
15  
16 unified mechanism for proteolysis and autocatalytic activation in the 20S proteasome. *Nat.*  
17  
18 *Commun.* **2016**, 7:10900.

19  
20 27. Vagin, A. A.; Steiner, R. A.; Lebedev, A. A.; Potterton, L.; McNicholas, S.; Long, F.;  
21  
22 Murshudov, G. N., REFMAC5 dictionary: organization of prior chemical knowledge and  
23  
24 guidelines for its use. *Acta Crystallogr. Sect. D - Biol. Crystallogr.* **2004**, 60, 2184-2195.

25  
26 28. Emsley, P.; Lohkamp, B.; Scott, W. G.; Cowtan, K., Features and development of Coot.  
27  
28  
29 *Acta Crystallogr. Sect. D - Biol. Crystallogr.* **2010**, 66, 486-501.  
30  
31  
32  
33  
34  
35  
36  
37  
38  
39  
40  
41  
42  
43  
44  
45  
46  
47  
48  
49  
50  
51  
52  
53  
54  
55  
56  
57  
58  
59  
60

Table 1. Chemical structures of compounds **4**, **6-36** and their inhibitory activity (apparent  $IC_{50}$  values) against  $\beta 2c$  and  $\beta 2i$  (determined by competitive ABPP). A high  $\beta 2i/\beta 2c$  ratio indicates selectivity for  $\beta 2c$ . Raw data used for calculations of  $IC_{50}$  values are in the Supplementary Information.

				Apparent $IC_{50}$ (nM)		Ratio
Compound	R <sub>3</sub>	R <sub>2</sub>	R <sub>1</sub>	$\beta 2i$	$\beta 2c$	$\beta 2i/\beta 2c$
<b>6</b>				106	23	5
<b>7</b>				6500	160	40
<b>8</b>				23	29	0.8
<b>9</b>				350	69	5
<b>10</b>				47	32	1
<b>11</b>				700	72	10
<b>12</b>				22	35	0.6
<b>13</b>				525	11	47
<b>14</b>				47	17	3

15				200	8	25
4 (LU-002c)				325	10	32
16				330	8	41
17				130	21	6
18			H	5900	26	224
19				1350	240	6
20				>1000	72	>14
21				61	47	1
22				540	18	30
23				204	210	1
24				325	380	0.8
25				>1000	280	>4
26				48040	2250	21
27				4100	510	8

<b>28</b>				>10000	3350	>3
<b>29</b>				260	35	7
<b>30</b>				280	11	25
<b>31</b>				200	31	7
<b>32</b>				360	43	8
<b>33</b>				175	41	4
<b>34</b>				170	17	10
<b>35</b>				45	16	3
<b>36</b>				420	40	11

**Table 2.** Apparent IC<sub>50</sub> values of compounds **1** (LU-102), **4**, **7**, **13**, **16**, **18**, **20**, **22** and **25** for the six catalytic sites from human cCPs and iCPs in Raji cell lysates, as established by competitive ABPP.

Compound	Apparent IC <sub>50</sub> (μM)						Ratio				
	β2c	β2i	β5c	β5i	β1c	β1i	β2i/β2c	β1i/β2c	β1c/β2c	β5i/β2c	β5c/β2c
<b>1</b> (LU-102)	0.013	0.020	1.33	1.17	>100	>100	2	>7700	>7700	90	102
<b>4</b> (LU-002c)	0.0050	0.14	1.3	2.8	>100	>100	27	>19000	>19000	540	250
<b>7</b>	0.17	2.9	>100	>100	>100	>100	17	>600	>600	>600	>600

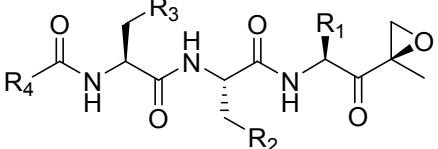
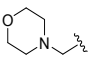
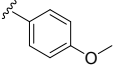
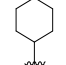
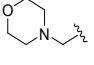
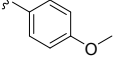
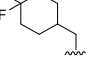
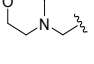
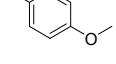
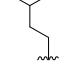
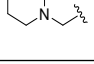
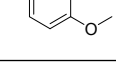
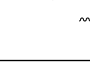
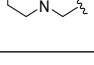
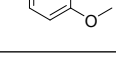
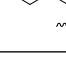
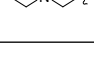
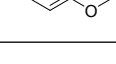
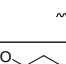
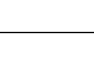
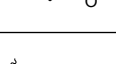
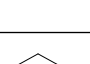
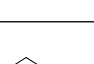
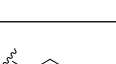
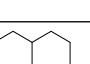
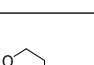
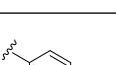
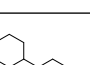
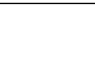
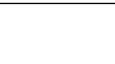
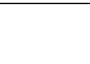
13	0.0060	0.23	1.4	2.2	>100	>100	40	>17000	>17000	380	241
16	0.0070	0.11	0.75	2.1	>100	>100	16	>14000	>14000	300	107
18	0.046	2.5	8.6	12.7	>100	>100	54	>2200	>2200	187	276
20	0.077	4.0	45.3	57.1	>100	>100	52	>1300	>1300	740	590
22	0.065	0.42	>100	>100	>100	>100	6	>1500	>1500	>1500	>1500
25	0.44	3.1	>100	>100	>100	>100	7	>220	>220	>220	>220

**Table 3.** Inhibition of proteasome activities by compounds **1** (LU-102), **4** (LU-002c), **7**, **13**, **16** (LU-012c), **18**, **20**, **22** and **25** in intact RPMI-8226 cells.

Compound	Apparent IC <sub>50</sub> (μM)						Ratio
	β2c	β2i	β5c	β5i	β1c	β1i	β2i /β2c
<b>1</b> (LU-102)*	0.29	0.41	>10	>10	>10	>10	1.4
<b>4</b> L(U-002c)*	1.80	>10	>10	>10	>10	>10	>5.6
<b>7</b>	>10	>10	>10	>10	>10	>10	n.d.
<b>13</b>	2.00	>10	>10	>10	>10	>10	>5
<b>16</b> (LU-012c)	1.250	>10	>10	>10	>10	>10	>8
<b>18</b>	>10	>10	>10	>10	>10	>10	n.d.
<b>20</b>	>10	>10	>10	>10	>10	>10	n.d.
<b>22</b>	>10	>10	>10	>10	>10	>10	n.d.
<b>25</b>	>10	>10	>10	>10	>10	>10	n.d.

\*Data cited from literature. n.d. not determined.

**Table 4.** Structures of compounds **5**, **37-53** and their inhibitory activity (apparent  $IC_{50}$  values) against  $\beta 2c$  and  $\beta 2i$  (determined by the competitive ABPP assay). A high  $\beta 2c/\beta 2i$  ratio indicates selectivity for  $\beta 2i$ .

					Apparent $IC_{50}$ (nM)		Ratio
Compound	R <sub>4</sub>	R <sub>3</sub>	R <sub>2</sub>	R <sub>1</sub>	$\beta 2c$	$\beta 2i$	$\beta 2c/\beta 2i$
<b>37</b>		H			>10000	>10000	n.d.
<b>38</b>		H			>10000	5530	>2
<b>39</b>		H			>10000	215	>46
<b>40</b>		H			>10000	8400	n.d.
<b>41a</b>		H			>10000	5000	>2
<b>41b</b>		H			6400	265	24
<b>42</b>		H			>10000	2750	>3
<b>5, LU002i</b>		H			>10000	320	>31
<b>43</b>		H			>10000	2800	>3
<b>44a*</b>		H			>10000	>10000	n.d.

44b*		H			915	100	9
45		H			>10000	>10000	n.d.
46					4250	4850	1
47					39	13	3
48					97	73	1
49					850	290	3
50					350	97	3
51					230	210	1
52					2300	3600	0.6
53					1150	3100	0.4

n.d. not determined. \*Compounds **44a** and **44b** are diastereomers; for details on stereochemistry see Supporting Information.

**Table 5.** Apparent IC<sub>50</sub> (μM) values of compounds **5** and **39** against the six catalytic active sites from human cCPs and iCPs, as determined in Raji cell lysate by competitive ABPP.

compound	β2i	β2c	β5i	β5c	β1i	β1c	Ratio β2c/β2i	Ratio β5c/β5i
----------	-----	-----	-----	-----	-----	-----	------------------	------------------



<b>5</b> (LU-002i)	0.18	12.1	>100	>100	>100	>100	67	~1
<b>39</b>	0.057	2.5	0.046	5.0	>100	>100	44	109

**Table 6.** Apparent IC<sub>50</sub> (μM) values of compounds **68**, **71**, **74**, **77**, **86** and **87** against the six catalytic active sites from human cCPs and iCPs, determined in Raji cell lysate by competitive ABPP.

compound	β2i	β2c	β5i	β5c	β1i	β1c
<b>68</b>	>100	>100	>100	>100	>100	>100
<b>71</b>	2.5	>100	>100	>100	>100	>100
<b>74</b>	12.0	>100	>100	>100	>100	>100
<b>77</b>	0.38	28	>100	>100	>100	>100
<b>86</b>	34.0	>100	>100	>100	>100	>100
<b>87</b>	0.19	19	28.40	>100	>100	53

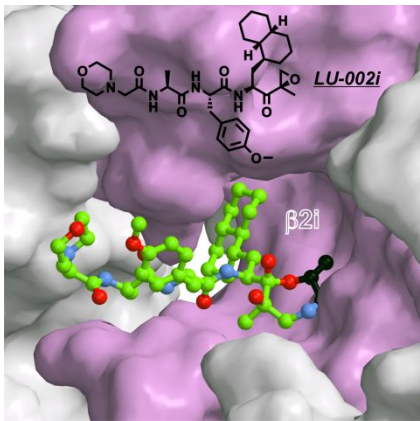


Table of Contents Graphic